

TOWARD FOUNDATION MODEL FOR MULTIVARIATE WEARABLE SENSING OF PHYSIOLOGICAL SIGNALS

Yunfei Luo^{1,*}, Yuliang Chen^{1,*}, Asif Salekin², Tauhidur Rahman¹

¹Halcioğlu Data Science Institute, University of California San Diego

²Schools of Engineering, Arizona State University

ABSTRACT

Time-series foundation models have the ability to run inference, mainly forecasting, on any type of time series data, thanks to the informative representations comprising waveform features. Wearable sensing data, on the other hand, contain more variability in both patterns and frequency bands of interest and generally emphasize more on the ability to infer healthcare-related outcomes. The main challenge of crafting a foundation model for wearable sensing physiological signals is to learn generalizable representations that support efficient adaptation across heterogeneous sensing configurations and applications. In this work, we propose NORMWEAR, a step toward such a foundation model, aiming to extract generalized and informative wearable sensing representations. NORMWEAR has been pretrained on a large set of physiological signals, including PPG, ECG, EEG, GSR, and IMU, from various public resources. For a holistic assessment, we perform downstream evaluation on 11 public wearable sensing datasets, spanning 18 applications in the areas of mental health, body state inference, biomarker estimations, and disease risk evaluations. We demonstrate that NORMWEAR achieves a better performance improvement over competitive baselines in general time series foundation modeling. In addition, leveraging a novel representation-alignment-match-based method, we align physiological signals embeddings with text embeddings. This alignment enables our proposed foundation model to perform zero-shot inference, allowing it to generalize to previously unseen wearable signal-based health applications. Finally, we perform nonlinear dynamic analysis on the waveform features extracted by the model at each intermediate layer. This analysis quantifies the model’s internal processes, offering clear insights into its behavior and fostering greater trust in its inferences among end users. The code is available: <https://github.com/Mobile-Sensing-and-UbiComp-Laboratory/NormWear>.

1 INTRODUCTION

Mobile and wearable sensors have been shown to be valuable for the field of healthcare by passively and continuously tracking physiological signals such as photoplethysmography (PPG) for pulse, electrocardiography (ECG) for heart activity, galvanic skin response (GSR), and electroencephalography (EEG) for brain activity. These time series signals are beneficial for early diagnosis, personalized health insights, and remote patient monitoring (Zhang et al., 2024a).

Recently, various foundation models on time series have been proposed (Ansari et al., 2024; Abbaspourzad et al., 2023; Woo et al., 2024; Foumani et al., 2024). Another common approach for signal modeling involves converting raw signal series into 2D images or spectrograms, using fixed-size sliding windows, followed by the use of visual encoders like Vision Transformers (ViT) to extract representations for making inferences (Semenoglou et al., 2023; Wimmer & Rekabsaz, 2023; Vishnupriya & Meenakshi, 2018; Chun et al., 2016; Krishnan et al., 2020; Dosovitskiy et al., 2020). These works have significantly advanced the field and provided valuable insights, yet two main issues still exist which need further exploration to fully understand their potential in wearable scenarios. First, contrastive learning-based foundation models (Abbaspourzad et al., 2023) rely on a predefined set of input signal types, making them unsuitable when transferring to scenarios with different types and numbers of sensors. Second, while both time series foundation models (Ansari et al., 2024; Zhang et al., 2022; Woo et al., 2024) and spectral-based approaches (Semenoglou et al.,

*These authors contributed equally to this work.

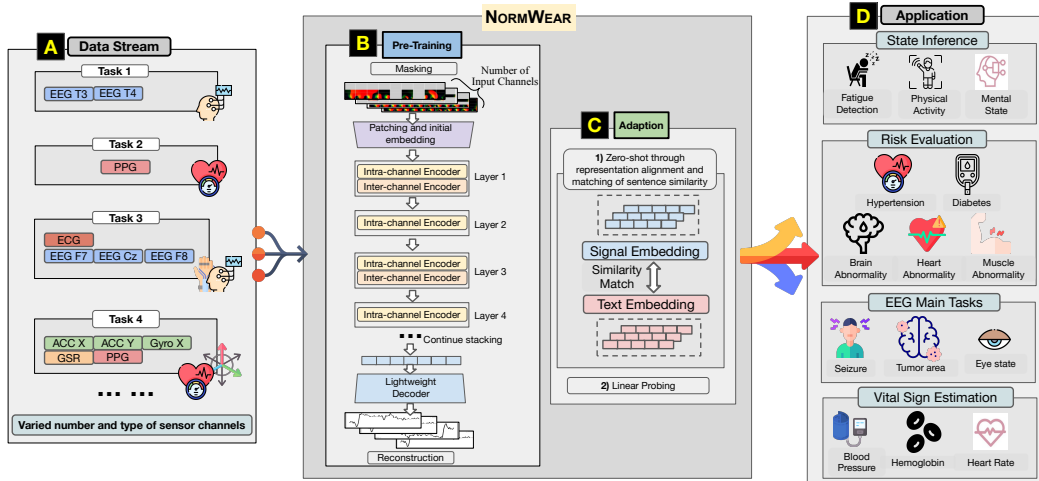


Figure 1: The role of our framework. Several icons from Freepik (n.d.); Zhang et al. (2024a.)

2023; Wimmer & Rekabsaz, 2023) attempt to address this issue by training a generic encoder that can handle type-agnostic series, they remain limited to processing only univariate series. Because of this constraint, these previous works fail to account for the heterogeneity of multivariate input data; specifically, they do not capture the complex relationships between signals from sensors located on different body parts. These two limitations of recent approaches hinder their generalization and usefulness for wearable health monitoring.

Moreover, Wearable-based multimodal physiological signals present unique challenges that distinguish them from general time series data, such as stock prices or weather patterns. Wearable signal modalities, such as PPG and EEG, vary in characteristics like dimensionality, sampling rate, and resolution, often requiring modality-specific preprocessing. Existing methods tokenize raw signals (Ansari et al., 2024; Zhang et al., 2022) or convert them into image or spectral representations (Wu et al., 2023; Mathew et al., 2024; Vaid et al., 2023). While effective for specific tasks, these approaches lack generalizability and fail to provide a consistent preprocessing pipeline across multiple modalities. A consistent framework that accommodates diverse signal requirements is essential for training deep learning-based foundation models and advancing multimodal signal analysis. Finally, digital healthcare applications emphasize model interpretability and robustness, which reveals an unignorable research gap in recent literature on studying the intrinsic behaviors of their proposed models.

In this work, we present NORMWEAR, a normative foundation model, aiming to learn effective wearable sensing representations, addressing the above-discussed research gaps. NORMWEAR has been pretrained on more than 2.5 million multivariate wearable sensing segments, comprising total of 14,943 hours of sensor signal series, using publically available datasets. We evaluated NORMWEAR on 18 public downstream tasks against competitive baselines under both linear probing and zero-shot inference. Overall, our contributions with the proposed NORMWEAR healthcare modeling framework can be summarized as follows:

- To our knowledge, we are the first to develop a foundation model specifically designed for wearable sensing data, capable of processing arbitrary configuration of multivariate signals from sources such as the heart, skin, brain, and physical body.
- NORMWEAR comprises novel methodologies built upon the advanced practice in both the fields of signal processing and deep learning, including (a) continuous wavelet transform (CWT) based multi-scale representations for modality- and number-agnostic tokenization, (b) channel-aware attention layer that enables the model to process arbitrary multivariate inputs, and (c) zero-shot inference with human sensing adapted fusion mechanism for improved efficacy.
- We are also the first to integrate and process a comprehensive wearable signals dataset with varied number of input channels for training self-supervised learning algorithms, with thorough downstream evaluation. These datasets cover key health applications, including mental and physical state inference, biomarker estimation, and disease risk evaluation. We make the preprocessed data, codebase, and model weights publicly available.

- We perform a comprehensive interpretability analysis and visualization to elucidate the model’s inner workings and decision-making processes, and we are the first to quantify the analysis with nonlinear-dynamic-analysis of the waveform features extracted by the models at each intermediate layer, offering insights into NORMWEAR’s neural activity patterns across various sensing signal types and tasks. This is crucial for validating the reliability of downstream applications and building trust with end users.

Our proposed NORMWEAR aims to provide a generalized data representation solution for smart health monitoring, benefiting the general public, and serving as a fundamental tool for researchers and professionals to address future healthcare challenges.

2 METHOD

Table 1: Downstream evaluation data. All these data are unseen during pretraining.

Downstream Dataset	Sensor	Tasks	#Samp. (#Subj.)
WESAD (Schmidt et al., 2018)	IMU, PPG, ECG, GSR	Stress Detection	11050(15)
UCI-HAR (Reyes-Ortiz et al., 2012)	IMU	HAR	10299(30)
DriverFatigue (Min et al., 2017)	EEG	Fatigue Detection	2400(12)
Activity Recognition Total	-	-	23749(57)
Epilepsy (Andrzejak et al., 2023)	EEG	State Recognize	11500(500)
GAMEEMO (Alakus et al., 2020)	EEG	Valence-Arousal	5600(28)
EEG Main Tasks Total	-	-	17100(528)
ECG-Abnormal (Bousseljot et al., 2009)	ECG	Abnormal Detection	11640(249)
PPG-BP (Liang et al., 2018)	PPG	Risk of Diseases	657(219)
PhysioNet EMG (Goldberger et al., 2000)	EMG	Muscular Diseases	163(3)
Risk Evaluation Total	-	-	12460(471)
Noninvasive-BP (Esmaili et al., 2017)	PPG	BP Estimate	125(26)
PPG-Hgb (Esmaili et al., 2017)	PPG	Hgb Estimate	68(68)
Fetal-fPCG (Bhaskaran et al., 2022)	PCG	Fetal HR Estimate	47(47)
Vital Signs Total	-	-	240(141)
Total All	-	-	53549(1197)

Table 2: Baselines and pretraining data.

Baseline Methods	Modeling Strategies	
TF-C (Zhang et al., 2022)	SoTA in TS SSL; modeling time and frequency domain information at same time.	
CLAP (Wu et al., 2023)	SoTA in audio modeling; process signal as spectrogram	
Chronos (Ansari et al., 2024)	SoTA in TS forecasting, leverage LLM for modeling	
Statistical approach	Reserve full interpretability	
Pretrain Dataset	Sensors	#Samp (hours).
Cuff-Less-BP (Kachuee et al., 2016)	ECG, PPG	42934(72)
PPG-Dalia (Reiss Attila, 2019)	ECG, PPG, IMU, GSR	42606(71)
Auditory-EEG (Alzahab et al., 2022)	EEG	13601(23)
PhyAAt (Bajaj et al., 2020)	EEG	19550(33)
MAUS (Beh et al., 2021)	ECG, PPG, GSR	13068(22)
Mendeleev-YAAD (Dar et al., 2022)	ECG, GSR	2964(5)
Brain-Cognitive (Dar et al., 2022)	EEG	51201(85)
EPHNOGRAM (Dar et al., 2022)	ECG, PCG	36611(61)
BIDMC (Dar et al., 2022)	ECG, PPG	8427(14)
Num Segments (# Segm.)	-	230,962(385)
# Segm. w/ Augment	-	2,576,418(4,294)
Num Sensor Signals (# Sign.)	-	802,019(1,337)
# Sign. w/ Augment	-	8,965,538(14,943)

2.1 DATASET CONSTRUCTION FOR MODEL PRE-TRAINING AND DOWNSTREAM EVALUATION

We curated a collection of 9 publicly available datasets (Table 2) exclusively for model pre-training, resulting in approximately 230,962 multivariate time series segments, comprising 385 hours of total sensor signal series. These datasets include signals from PPG, ECG, EEG, GSR, PCG, and IMU sensors. Each segment contains a variable number of input channels, depending on the signals available in each dataset. To address the dataset size limitation, we applied heuristic data augmentation (algorithm 1), expanding the pre-train dataset to 2.5 million segments, comprising 4,294 hours of sensor signal series. If each variate were treated individually, the dataset would consist of approximately 9 million univariate segments, covering a total of 14,943 hours. This large-scale and diverse dataset ensures sufficient coverage of various signal modalities and configurations, enhancing the model’s capacity to generalize across a wide range of sensor setups in downstream tasks.

To prevent potential data leakage in downstream tasks, we evaluate our model’s transferability using an additional 11 publicly available datasets encompassing 18 modeling tasks, which include affective state classification, physical state recognition, biological estimation, and disease risk evaluation. Details about the datasets is presented in Table 1.

2.2 TOKENIZATION

Tokenization is a fundamental term widely used in natural language processing. In the context of wearable sensing, we leverage this term to represent the stage of signal processing before sending the processed data to the deep learning-based encoder. Spectral methods, which utilize the short-time Fast Fourier Transform (FFT) (Brigham, 1988) with a sliding window to compute spectrograms, are widely regarded as the benchmark approach for tokenization. However, due to the inherent trade-off between time and frequency resolution, the spectral representation with a fixed window size

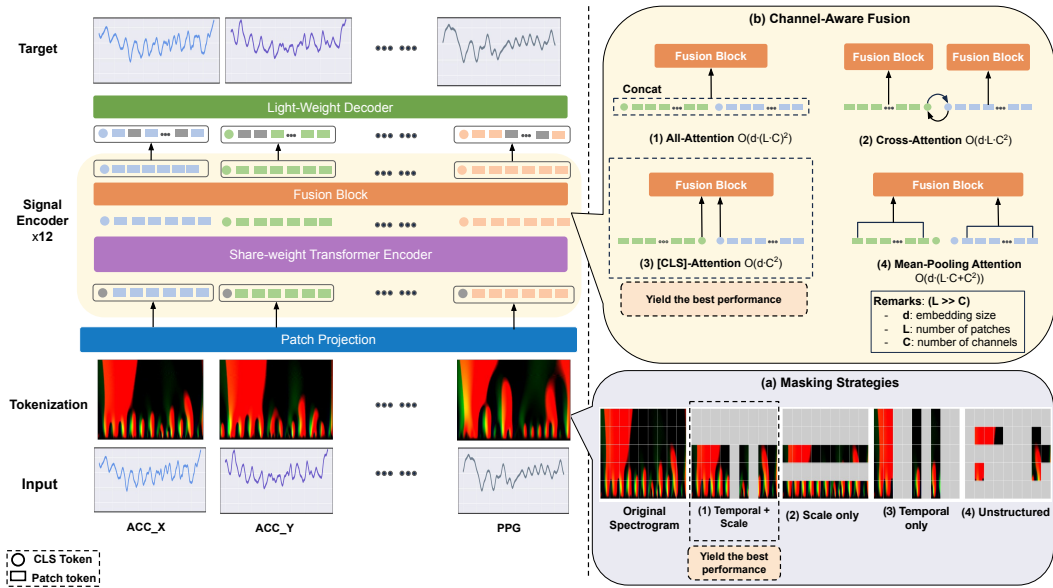


Figure 2: Overview of the pretrain pipeline.

cannot be generalized. This is because the window size has to be modulated accordingly when the modality varies. To enhance transferability, we propose a well-designed signal processing pipeline that preserves information in both the frequency and time domains across multiple scales. We begin by calculating the first and second derivatives for each single signal series, as suggested by Slapničar et al. (2019), followed by computing the continuous wavelet transform (CWT) on both the raw and derivative series, resulting in three scalograms. Then, we stack the three scalograms to form data in RGB-image-like format. The derivatives capture the rate of signal change at different moments, while the wavelet transform provides a multi-resolution encoding that preserves information from both the time and frequency domains Torrence & Compo (1998). For the wavelet transform, we use the Mexican Hat wavelet for signal convolution, as recommended by previous studies (Burke & Nador, 2004; Hosni & Atef, 2023; Hassani, 2021; Negi et al., 2024; Nedorubova et al., 2021b). We apply scales ranging from 1 to 64, following the guidance of (Sengupta et al., 2022; Nedorubova et al., 2021a), which sufficiently covers most frequency bands of interest for physiological signals. Finally, this RGB-like scalogram is divided into patches, which is treated in the same way as tokens in an ViT (Dosovitskiy et al., 2020). In this way, this tokenization approach can be applied to various types of sensing signals without sensor-specific adjustments or reconfigurations.

2.3 MODEL ARCHITECTURE AND PRE-TRAIN STRATEGIES

Following the tokenization step, we adopt common reconstruction-based pretraining strategies from Masked Auto Encoder (MAE) (He et al., 2021; Huang et al., 2023; Zhang et al., 2023a), which applying masking to input tokens and and optimizing the model using mean squared error (MSE) for reconstructing the raw time series. Inspired by Huang et al. (2023), we experiment with four masking strategies, as shown in Figure 2 (a), including masking on (1) temporal and scale, (2) scale only, (3) temporal only, and (4) unstructured axes. We observe that the temporal and scalar masking yields the best performance for the downstream tasks.

For the model architecture, we construct the backbone of our proposed framework with a convolutional patching layer followed by 12 standard Transformer blocks (Vaswani et al., 2023). For the same reason, NORMWEAR uses a lightweight decoder consisting of 2 Transformer blocks, combined with a linear projection layer and a convolution layer to reconstruct the raw physiological signals both temporally and spatially. We also prepend a special token [CLS] at each signal channel, aiming to learn and extract a generic representation for each signal.

Another important point to consider is that although empirical studies (Nie et al., 2023; Abaspourazad et al., 2023) show that channel-independent structures effectively capture local patterns, they fail to account for relationships across channels. To address this, we introduce a channel-aware attention (fusion) layer after every other encoder block to incorporate cross-channel information. We explore several fusion approaches as shown in Figure 2 (b), with each method described below:

(1) **All-Attention Fusion:** This approach involves concatenating all tokens from each modality without considering their individual properties and fusing the information through a self-attention module. However, this method requires quadratic computation time, as every token passes through the self-attention module, making it impractical for real-world applications.

(2) **Cross-Attention Fusion:** In addition to the cross-attention mechanism used in Cross-ViT (Chen et al., 2021), we introduce a slight modification to fit in our problem setting. We propose a symmetric fusion method, using the [CLS] token from each modality as an intermediary to exchange information between the patch tokens of another modality, then projecting the information back to its original modality in the subsequent Transformer layer. While this strategy is efficient, it restricts the model to handling only two time series signals or modalities, which deviates from our goal of building a general model capable of processing an arbitrary number of channels.

(3) **[CLS]-Attention Fusion** The [CLS] token serves as an abstract global representation for each signal modality. Here, we propose a hybrid fusion approach. We stack the [CLS] tokens from all signal modalities and perform feature fusion using a self-attention mechanism. The fused [CLS] token is then reattached to its original channel, enabling the newly learned information to be propagated to each patch token in subsequent transformer encoder layers.

(4) **Mean-Pooling Fusion** Similar to the [CLS]-Attention Fusion approach, we employ mean-pooling within each channel instead of using the [CLS] token as an abstract global representation.

Our empirical results show that [CLS]-attention fusion achieves the best performance for downstream tasks for our proposed NORMWEAR model. Details of all the ablation studies are reported in appendix D.

2.4 ZERO SHOT INFERENCE WITH MEMORY STREAM INSPIRED FUSION MECHANISM

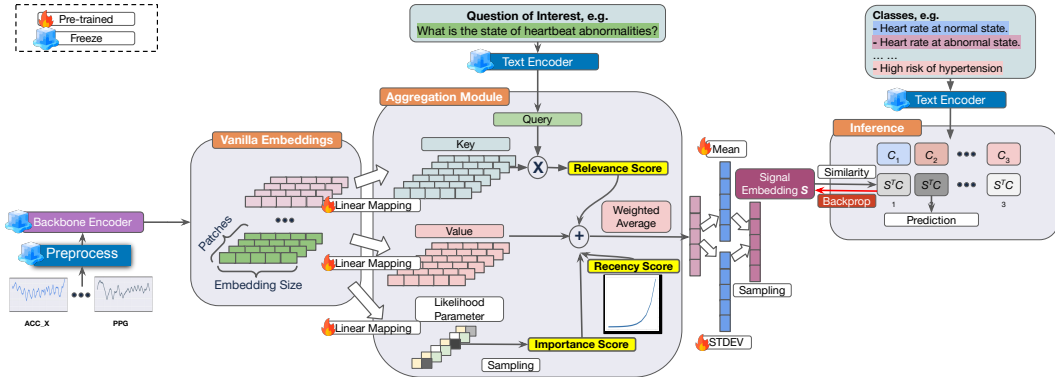


Figure 3: Memory stream inspired temporal fusion mechanism for representation alignment.

We enable zero-shot inference by introducing a novel temporal fusion mechanism that transforms multivariate sensing data into a unified representation within a text embedding space. Unlike prior approaches (Radford et al., 2021; Wu et al., 2023) that trained both signal encoder and text encoder jointly from scratch, our method is lightweight, as it does not require retraining these encoders.

For the objective of representation alignment specifically, with the semantic embedding of query sentence q and backbone output $H \in \mathbb{R}^{P \times E}$ where P is the patch size and E is the embedding size, we will have the final fused representation $f(q, H) = \hat{Y} \in \mathbb{R}^E$ which the fusion function f will be described in details in the following subsections. We then leverage the semantic embedding of ground truth sentence Y to supervise the fused output \hat{Y} with integrated loss function with penalty on Manhattan distance and cosine similarity, aiming to align the physiological representation with the same direction and magnitude as the semantic representation:

$$Loss(Y, \hat{Y}) = \lambda |Y - \hat{Y}| + \left(1 - \frac{Y \cdot \hat{Y}}{\|Y\| \|\hat{Y}\|} \right) \quad (1)$$

where λ is hyper-parameters controlling the weight of loss components. During pretraining on the pretraining datasets stated in Table 2, we introduce both classification and regression tasks, as well as data augmentation with multiple alternative sentence patterns for each paired datasets, in order to

allow the model to have a better estimation of the representation transformation function from the physiological signal space to the semantic space.

In this method, we leverage text as a common modality, mapping input signals into a unified textual space. By inferring within this shared space, we can assess the similarity between aligned physiological representations and potential ground-truth states, enabling zero-shot inference. However, relying solely on the cross-attention (relevance) score for temporal fusion is insufficient for human sensing tasks, as it overlooks temporal proximity, the contextual importance of each patch, and the intrinsic variations within each representation. Human sensing tasks, such as gesture recognition or physiological monitoring, often require prioritizing recent temporal patterns due to their stronger correlation with immediate human actions or conditions (Chowdhury et al., 2020; Chaudhury et al., 2021). To this end, we introduce recency scores, which assign higher weights to patches closer to the most recent time step in the sequence. Additionally, during vector aggregation, we adopt a variational-inspired approach (Kingma & Welling, 2022) where we compute the mean and standard deviation of patch embeddings before sampling. This design injects stochasticity into the representation, encouraging the model to explore and capture nuanced variations in human sensing data.

Memory stream inspired fusion mechanism (MSiTF). As mentioned above, the NormWear encoder have latent output shape of $H \in \mathbb{R}^{P \times E}$. Such an embedding vectors of all the patches have to be aggregated (average pooling by default) to form a fixed length representation suitable for non-sequential downstream tasks including classification or regression. Inspired by the philosophy of memory stream retrieval from the design of virtual game characters in Park et al. (2023), we implemented a novel fusion mechanism named MSiTF to generate representations optimized for human sensing, shown in Figure 3. Intuitively, MSiTF fuses the latent representations from all time steps before the final output layer with weighted scores computed according to **(1) how relevant they are to the objective tasks**, **(2) how important they are to the data itself**, and **(3) how close they are to the most current time step**. The output layer is instructed to select the most informative representations to optimize the objective task of representation alignment.

As outlined in Figure 3, we consider the *Relevance* score to be the cross-attention score between the sentence embedding generated by the pretrained language model (Muzammil, 2021) of the query sentence and the key representation of the embedding of each time step. For the *Recency* score, we use an exponential decay function, where the further the time step to the most recent time step, the lower the score. Finally, we consider the importance score IMP in this case to be whether to keep the representation at each time step or not. In order to achieve this, we assign binary parameters to each time step, denoted as $\theta_t = p(v_t) \in \mathbb{R}^2$ where $v_t \in \mathbb{R}^E$ is the representation vector at time step t and p is a trainable linear transformation function which will be optimized during pretraining. We then have the importance score for each patch defined as

$$W_{imp}(t) = \arg \max_{i \in \{0,1\}} \frac{\exp \left(\left(\log(\theta_{t,i}) + \epsilon \right) / \tau \right)}{\sum_{j \in \{0,1\}} \exp \left(\left(\log(\theta_{t,j}) + \epsilon_j \right) / \tau \right)} \quad (2)$$

where ϵ is the noise term sampled from Gumbel distribution (Jang et al., 2017), and τ is the temperature controlling the sharpness of the softmax function. Because $\arg \max$ is not a differentiable function, we will directly take the resulting probability corresponding to index at $j = 1$ to be the *importance* score, with τ being set to a small number to push the result closer to one hot vector from the softmax function. As a result, the trainable linear transformation will be optimized to determine whether to activate the gate during forward pass on each input signals. The final score for each patch is the summation of the three scores as described above. This score will be treated as the weight for aggregating the representations from all the patches to form the fixed length embeded output (vector with size of 768 in our case). This aggregated vector is then passed to the successive tasks on representation alignment and downstream task inference.

3 EXPERIMENTS

In this section, we present a comprehensive evaluation across 11 publicly available datasets, focusing on 18 widely-recognized digital healthcare tasks. We first assess the transferability advantage of our proposed model compared to the solid baselines. Additionally, we examine the zero-shot capabilities of *NormWear*. Finally, we conduct nonlinear dynamics analysis on the waveform features across intermediate encoder layer to inspect model’s behaviors.

3.1 SELECTION OF BASELINES COVERING REPRESENTATIVE MODELING STRATEGIES

Modeling multivariate wearable signals with arbitrary input channels and sensor types, such as those capturing activities of heart, brain, and body physical motions, presents unique challenges, as no universally recognized open-source baseline or state-of-the-art (SoTA) model exists in this domain. To evaluate our approach, we selected diverse and representative baselines (as shown in Table 2).

In the literature, different modeling strategies have been proposed. Firstly, early approaches involved handcrafting statistical features, which was a widely adopted practice in signal processing (Yan et al., 2023a; Reyes-Ortiz et al., 2012; Mikelsons et al., 2017). We include this simple baseline as sanity check. Secondly, since sensory data can be naturally represented as time series (Woo et al., 2024; Semenoglou et al., 2023), we benchmarked our model against Chronos (Ansari et al., 2024), as well as the common self-supervised framework TF-C (Zhang et al., 2022). Finally, the spectrum-based modeling methods (Vishnupriya & Meenakshi, 2018; Chun et al., 2016; Krishnan et al., 2020) are widely used for signal modeling. Therefore, we incorporate CLAP (Wu et al., 2023) into baselines that has demonstrates SoTA performance in spectrogram-based modeling. These baselines span distinct paradigms, providing a solid foundation to demonstrate the strengths of our model in wearable signal tasks.

3.2 DOWNSTREAM EVALUATION, NORMWEAR ACHIEVES THE PEAK PERFORMANCE

We perform supervised training to evaluate the representation with linear probing on each downstream dataset. Performance is then assessed in the test set of these datasets. The classification tasks, using logistic regression, are solved by Newton’s method with conjugate gradient, with AUC ROC being reported as main metric. The regression (vital signs) tasks, using ridge regression, are solved by Cholesky’s method with closed form solution, with relative accuracy being reported. All scores are the higher the better.

From Figure 5, Table 3, and Table 4, we observe that NormWear consistently achieves peak performance across all task groups, including activity recognition, EEG signal analysis, disease risk evaluation, and vital sign estimation. Furthermore, its leading performance remains consistent across various evaluation metrics. Based on the macro-averaged total score across task groups, NormWear delivers a 3.6% improvement over the state-of-the-art (SoTA) time-series self-supervised learning framework, a 5.3% improvement over the SoTA spectrum-based modeling method, a 5.6% improvement over SoTA time-series forecasting models with LLM backbones, and a 5.3% improvement over standard statistical baselines. On larger datasets, NormWear significantly outperforms the statistical baseline by 9.0% and 7.5% for activity recognition and EEG brain activity monitoring tasks, respectively. On smaller datasets, it still achieves peak performance in disease risk evaluation. For vital sign estimation, all methods yield comparable results, suggesting inherent challenges in these regression tasks that warrant further investigation but are beyond the scope of this study.

These findings illustrate NormWear’s capacity to balance consistency and adaptability across a diverse range of tasks and conditions. By excelling across standard benchmarks while addressing the intricacies of varied applications, NormWear exemplifies the philosophy of a foundation model: a reliable generalist capable of performing robustly across both typical and challenging scenarios.

3.3 SCALING UP THE PRETRAINING DATA SIZE

In addition to demonstrating that NormWear outperforms all strong baselines, we further investigate the effect of varying pretraining data size on the model’s downstream performance to examine whether the scaling law applies to our proposed methodology. As shown in Figure 4, the overall performance (measured by accuracy) significantly improves as the pretraining data size increases from approximately 37k (62 hours) to nearly 2.5M (4000 hours) samples of wearable signal data. This observation indicates that our model adheres to the scaling law, highlighting its potential scalability and suitability for future large-scale applications.

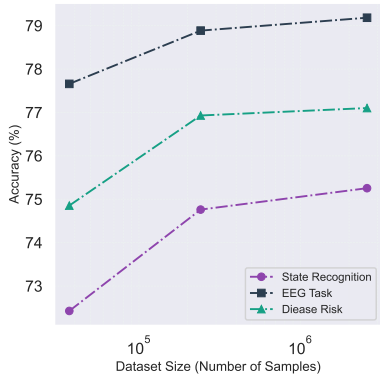


Figure 4: Scaling on downstream tasks.

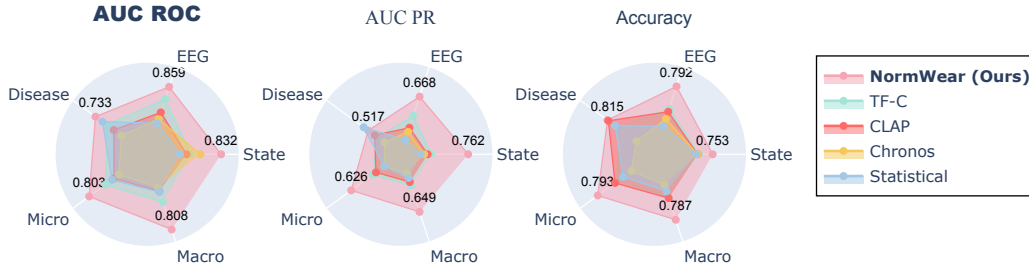


Figure 5: Overview of performance trend of NormWear against competitive baselines in downstream tasks: (1) **Disease** risk predictions. (2) **EEG** main tasks (mental and abnormal states prediction). (3) **State** recognition: physical and mental activities. (4) **Macro**: Average performance over types of tasks. (5) **Micro**: Average performance over each task.

Table 3: Performance on various downstream wearable-signal-based health related applications under linear probing evaluation.

Downstream Tasks	Statistical	Chronos	CLAP	TF-C	NormWear (Ours)
WESAD	66.213	71.489	72.383	69.865	75.390
UCI-HAR	95.784	91.593	96.420	96.892	98.928
DriverFatigue	63.249	76.722	61.889	66.882	75.167
Activity Recognition Avg.	75.082	79.935	76.897	77.880	83.162
Epilepsy (eye open)	82.489	82.41	85.094	89.153	92.203
Epilepsy (eye close)	87.457	88.218	89.867	94.416	94.908
Epilepsy (health area)	86.274	81.08	83.711	85.619	88.117
Epilepsy (tumor area)	82.816	81.034	83.644	86.348	86.888
Epilepsy (seizure)	88.272	97.572	97.734	93.998	96.638
GAMEEMO	51.009	53.747	52.551	56.275	56.532
EEG Main Tasks Avg.	79.720	80.677	82.100	84.302	85.881
ECG-Abnormal	97.092	98.585	97.23	98.275	99.041
PPG-BP (HTN)	59.499	52.425	56.757	65.229	60.344
PPG-BP (DM)	47.823	51.164	42.455	57.883	59.459
PPG-BP (CVA)	71.25	50.278	51.667	58.125	70.278
PPG-BP (CVD)	51.219	58.31	50.91	58.674	52.596
PhysioNet EMG	99.309	61.6	98.627	78.308	98.184
Risk Evaluation Avg.	71.032	62.060	66.274	69.416	73.317
Noninvasive-BP	92.31	91.79	91.922	87.481	92.470
PPG-Hgb	94.219	95.005	94.291	93.408	94.766
Fetal-fPCG	98.929	99.048	99.195	99.077	99.088
Vital Signs Avg.	95.153	95.281	95.136	93.322	95.441
Micro Avg.	78.623	76.782	78.130	79.773	82.833
Macro Avg.	80.247	79.488	80.103	81.230	84.450

3.4 THE FIRST ZERO-SHOT ENABLED FOUNDATION MODEL FOR WEARABLE SENSING HEALTH APPLICATIONS

We achieve zero-shot inference by pretraining our proposed novel temporal fusion module on the task of representation alignment following the guidance in (Zhang et al., 2024a; Liu et al., 2024) to map the embedding from our proposed foundation model to semantic space. During test-time inference on downstream datasets, each ground truth label is converted into a sentence (details in appendix. B), which is transformed into a text embedding using a frozen text encoder. The sentence with the closest distance with the embedding from our foundation model is used as the final inferential result. We also include the SoTA spectral-based model CLAP Wu et al. (2023) as a baseline to provide a more comprehensive comparison of the results. For CLAP, we experimented with both Manhattan distance (MD) and dot product (DP) as similarity metrics during inference. From table 5, we could observe that overall, the models equipped with our temporal proposed novel fusion mechanism outperform the baselines including leveraging the vanilla attention fusion mechanism. Although the final performance may not surpass that of linear probing, our work offers a significant contribution as an initial attempt to enable zero-shot inference through a lightweight pipeline across various wearable sensing healthcare tasks, without the need to rely on existing generative language

Table 4: Details of Incidental Performance Metrics.

Task Group	Methods	AUC ROC	AUC PR	Accuracy	Precision	Recall	F1 Score
Activity Recognition	Statistical	75.082	63.996	65.298	61.450	61.56	61.034
	Chronos	79.935	65.622	66.175	62.044	61.512	60.522
	CLAP	76.897	67.026	66.349	62.790	62.826	62.435
	TF-C	77.880	68.228	67.175	64.967	64.798	64.783
	NormWear (Ours)	83.162	76.232	75.254	72.606	72.177	72.053
EEG Main Tasks	Statistical	79.720	50.172	73.921	63.567	57.529	57.948
	Chronos	80.677	55.507	75.285	72.442	52.520	47.671
	CLAP	82.100	57.518	76.391	68.506	61.961	62.650
	TF-C	84.302	61.864	76.825	71.702	65.517	67.889
	NormWear (Ours)	85.881	66.841	79.182	72.485	69.158	69.698
Disease Risk Evaluation	Statistical	71.032	53.783	79.688	52.718	53.235	50.807
	Chronos	62.060	40.673	71.910	45.512	43.739	40.569
	CLAP	66.274	48.232	81.327	53.028	54.721	52.804
	TF-C	69.416	46.312	78.929	52.123	52.352	51.349
	NormWear (Ours)	73.317	51.666	81.530	54.133	56.314	54.428
Micro Average	Statistical	75.317	51.596	74.503	58.804	56.618	55.709
	Chronos	73.082	51.596	72.113	59.590	50.806	47.401
	CLAP	74.729	55.705	76.357	61.171	59.238	58.669
	TF-C	77.063	56.916	75.737	62.523	60.107	60.652
	NormWear (Ours)	80.312	62.649	79.336	65.168	64.624	64.061
Macro Average	Statistical	75.278	55.983	72.969	59.245	57.441	56.596
	Chronos	74.224	53.934	71.123	59.999	52.590	49.587
	CLAP	75.091	57.592	74.689	61.441	59.836	59.296
	TF-C	77.199	58.801	74.310	62.931	60.889	61.340
	NormWear (Ours)	80.787	64.913	78.656	66.408	65.883	65.393

Table 5: Zero-shot performance on the downstream datasets, with AUC ROC being reported. The last two columns show the average across the tasks and across group types respectively.

Model	WESAD	UCI-HAR	DriverFatigue	GAMEEMO	Epilepsy (eye open)	Epilepsy (eye close)	Epilepsy (health area)	Epilepsy (tumor area)	Epilepsy (seizure)	PPG-BP (HTN)	PPG-BP (DM)	PPG-BP (CVA)	PPG-BP (CVD)	ECG-Abnormal	PhysioNet EMG	Micro Avg.	Macro Avg.
CLAP - MD	45.3	62.8	58.5	53.1	44.9	45.1	47.6	30.5	84.9	59.4	41.8	46.0	57.4	22.9	55.4	50.4	51.2
CLAP - DP	50.7	52.3	61.1	51.6	54.4	41.9	58.6	46.4	74.3	52.2	41.4	50.6	58.9	42.7	38.3	51.7	52.2
NORMWEAR w/ MSITF	55.9	71.4	54.9	50.2	54.0	56.4	66.9	57.4	53.7	56.5	53.2	65.0	63.1	74.3	65.7	59.9	60.1
- w/o IMP	56.2	70.3	55.4	49.8	54.0	56.5	66.9	57.3	52.9	56.5	54.3	61.7	60.7	73.4	65.2	59.4	59.6
- w/o text aug	54.8	65.8	55.2	49.2	31.0	58.4	58.6	32.8	58.1	50.2	52.6	50.8	50.6	47.7	33.6	50.0	51.4

models. We present this outcome to demonstrate that, even without fine-tuning, the model is capable of learning informative representations that can be directly leveraged for downstream tasks. Furthermore, as shown in Section 3.2, even a straightforward adaptation, such as linear probing, can yield notably improved results.

3.5 QUANTIFY THE OBSERVED INTRINSIC BEHAVIORS: NONLINEAR DYNAMICS ANALYSIS ON THE FEATURES FROM EACH LAYER

Understanding the representations extracted by intermediate layers is crucial to interpreting our model’s behavior. To quantify the meaningfulness of these representations, we conducted a nonlinear dynamics analysis inspired by chaos theory. This method analyzes the features’ intrinsic behaviors through metrics like the Lyapunov exponent (Wolf et al., 1985) (sensitivity to initial conditions), Hurst exponent (Qian & Rasheed, 2004) (self-correlation/seasonality), and persistence entropy (Yan et al., 2023b) (unpredictability in system states). We obtain the following key observations:

1. Deeper Layers Capture Higher-Order Complexity.

- For signals such as GSR, EEG, and ACC, deeper layers show lower self-correlation (DFA (Hu et al., 2001)) and higher unpredictability (persistence entropy), indicating a transition to representations that are less periodic and more chaotic.
- The decrease in the Lyapunov exponent across layers suggests reduced variation in extracted features, aligning with the idea that deeper layers capture more abstract, long-term patterns with broader receptive fields.

2. Modalities with Simpler Dynamics. In contrast, PPG and ECG signals, dominated by regular heart activity, exhibit more stable patterns across layers. This aligns with their simpler waveform structures and less complex dynamics compared to signals related to neural and physical activities.

These visualizations reveal that the model progressively transforms raw sensory data into representations aligned with the complexity of each signal. For GSR and EEG, deeper layers exhibit increased unpredictability and reduced periodicity, highlighting the extraction of nuanced, higher-order patterns critical for human sensing. In contrast, the stability of representations for PPG and ECG reflects their simpler dynamics, demonstrating the model’s adaptability to varying signal characteristics. This analysis confirms that the intermediate representations are purposefully optimized to capture the temporal and structural nuances of each modality, supporting the conclusion that the model learns meaningful features tailored to human sensing tasks.

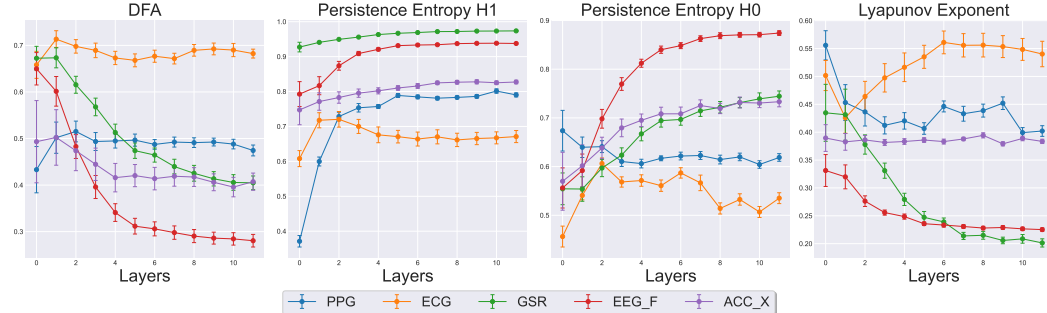


Figure 6: Nonlinear dynamic analysis on the waveforms extract at different layers of our model.

4 LIMITATIONS AND CONCLUSION

In this work, we mainly propose a foundation model for wearable physiological signals. There are three main limitations. Firstly, for the representation alignment pipeline, although we make significant efforts to augment the text data and add a variational sampling mechanism, we have a relatively limited set of wearable sensing-based healthcare objectives during pretraining. Drawing insights from the natural language processing domain (Devlin et al., 2019), we encourage future studies to increase the diversity of tasks for pretraining to achieve a more promising performance. Secondly, regarding zero-shot inference, the current pipeline design of NORMWEAR is more aligned with a classification scenario, also as suggested in Wu et al. (2023) and Zhang et al. (2024b). The most straightforward approach for regression would be to discretize the target label into bins. However, this approach does not fully address the challenge of adapting to regression tasks. Therefore, we recommend exploring alternative modeling strategies for performing zero-shot learning on continuous scales. Finally, human sensing includes signals from a wide range of frequency bands. For example, audio or radar data, as one of the popular modalities in contactless sensing, has a much higher and wider range of frequencies of interest. In contrast, lower-frequency data are more common in clinical research. For instance, most wearable devices record only minute-to-minute data such as heart rate, estimated calories consumed, and noise level around. Medical-related bio-markers are day-to-day data such as measurements of glucose level, blood pressure, and estimated body fat. In the current design, NORMWEAR does not incorporate such a wide variety of frequency ranges; however, there is great potential to verify and improve its ability when extending to other type of signals with a wider range of frequency bands of interest, which is a future research scope.

In conclusion, NORMWEAR is a practical tool that could serve as a starting point for researchers and clinicians when tackling a problem with wearable sensing based signal data. Our proposed model could extract informative embedding representations from raw signal series, which can be leveraged for further machine learning modeling, clustering, embedding vector-based information retrieval, and deployment of real-time health states monitoring with minimal tuning. We’ve justified the utilizability and generalization of NORMWEAR through an extensive evaluation of various ubiquitous health applications. Along with the interpretability analysis, our work could provide a transparent understanding of the model’s inner feature extraction and importance assignment processing. As for future works, it is important to leverage our proposed model on more large scale clinical applications and explore the applicability of embedding vectors as state representations for intervention modeling problems that comprise the decision-making process. We also suggest extending the proposed model on contactless sensing signals, as mentioned previously, such as audio and thermal imaging, which could provide more thorough health-related information.

ETHICS STATEMENT

This study contains applications in the field of healthcare. We ensured that all the data being used during pretraining and evaluations were made publicly available by the original authors, and all these works were cited properly.

REPRODUCIBILITY STATEMENT

The full code base, comprising all the code and documentation required for model construction, pretraining, downstream evaluation, and reproduction of the experimental results, is published at <https://github.com/Mobile-Sensing-and-UbiComp-Laboratory/NormWear>.

REFERENCES

- Salar Abbaspourazad, Oussama Elachqar, Andrew C Miller, Saba Emrani, Udhyakumar Nallasamy, and Ian Shapiro. Large-scale training of foundation models for wearable biosignals. *arXiv preprint arXiv:2312.05409*, 2023.
- Talha Burak Alakus, Murat Gonen, and Ibrahim Turkoglu. Database for an emotion recognition system based on eeg signals and various computer games–gameemo. *Biomedical Signal Processing and Control*, 60:101951, 2020.
- Nibras Abo Alzahab, Angelo Di Iorio, Luca Apollonio, Muaaz Alshalak, Alessandro Gravina, Luca Antognoli, Marco Baldi, Lorenzo Scalise, and Bilal Alchalabi. Auditory evoked potential eeg-biometric dataset, 2022.
- Ralph Gregor Andrzejak, Klaus Lehnertz, Christoph Rieke, Florian Mormann, Peter David, and Christian E. Elger. Indications of nonlinear deterministic and finite-dimensional structures in time series of brain electrical activity: Dependence on recording region and brain state [dataset]. *Physical Review E*, 2023. doi: 10.34810/data490. URL <https://doi.org/10.34810/data490>.
- Abdul Fatir Ansari, Lorenzo Stella, Caner Turkmen, Xiyuan Zhang, Pedro Mercado, Huibin Shen, Oleksandr Shchur, Syama Sundar Rangapuram, Sebastian Pineda Arango, Shubham Kapoor, et al. Chronos: Learning the language of time series. *arXiv preprint arXiv:2403.07815*, 2024.
- Nikesh Bajaj, Jesús Requena Carrión, and Francesco Bellotti. Phyaat: Physiology of auditory attention to speech dataset. *arXiv preprint arXiv:2005.11577*, 2020.
- Win-Ken Beh, Yi-Hsuan Wu, and An-Yeu (Andy) Wu. Maus: A dataset for mental workload assessment on n-back task using wearable sensor, 2021. URL <https://dx.doi.org/10.21227/q4td-yd35>.
- Amrutha Bhaskaran, Sidhesh Kumar J, Shirley George, and Manish Arora. Heart rate estimation and validation algorithm for fetal phonocardiography. *Physiological Measurement*, 43(7):075008, jul 2022. doi: 10.1088/1361-6579/ac7a8c. URL <https://dx.doi.org/10.1088/1361-6579/ac7a8c>.
- Rishi Bommasani, Drew A. Hudson, Ehsan Adeli, Russ Altman, Simran Arora, Sydney von Arx, Michael S. Bernstein, Jeannette Bohg, Antoine Bosselut, Emma Brunskill, Erik Brynjolfsson, Shyamal Buch, Dallas Card, Rodrigo Castellon, Niladri Chatterji, Annie Chen, Kathleen Creel, Jared Quincy Davis, Dora Demszky, Chris Donahue, Moussa Doumbouya, Esin Durmus, Stefano Ermon, John Etchemendy, Kawin Ethayarajh, Li Fei-Fei, Chelsea Finn, Trevor Gale, Lauren Gillespie, Karan Goel, Noah Goodman, Shelby Grossman, Neel Guha, Tatsunori Hashimoto, Peter Henderson, John Hewitt, Daniel E. Ho, Jenny Hong, Kyle Hsu, Jing Huang, Thomas Icard, Saahil Jain, Dan Jurafsky, Pratyusha Kalluri, Siddharth Karamcheti, Geoff Keeling, Fereshthe Khani, Omar Khattab, Pang Wei Koh, Mark Krass, Ranjay Krishna, Rohith Kuditipudi, Ananya Kumar, Faisal Ladhak, Mina Lee, Tony Lee, Jure Leskovec, Isabelle Levent, Xiang Lisa Li, Xuechen Li, Tengyu Ma, Ali Malik, Christopher D. Manning, Suvir Mirchandani,

-
- Eric Mitchell, Zanele Munyikwa, Suraj Nair, Avanika Narayan, Deepak Narayanan, Ben Newman, Allen Nie, Juan Carlos Niebles, Hamed Nilforoshan, Julian Nyarko, Giray Ogut, Laurel Orr, Isabel Papadimitriou, Joon Sung Park, Chris Piech, Eva Portelance, Christopher Potts, Aditi Raghunathan, Rob Reich, Hongyu Ren, Frieda Rong, Yusuf Roohani, Camilo Ruiz, Jack Ryan, Christopher Ré, Dorsa Sadigh, Shiori Sagawa, Keshav Santhanam, Andy Shih, Krishnan Srinivasan, Alex Tamkin, Rohan Taori, Armin W. Thomas, Florian Tramèr, Rose E. Wang, William Wang, Bohan Wu, Jiajun Wu, Yuhuai Wu, Sang Michael Xie, Michihiro Yasunaga, Jiaxuan You, Matei Zaharia, Michael Zhang, Tianyi Zhang, Xikun Zhang, Yuhui Zhang, Lucia Zheng, Kaitlyn Zhou, and Percy Liang. On the opportunities and risks of foundation models, 2022. URL <https://arxiv.org/abs/2108.07258>.
- Ralf Boussejot, Dieter Kreisel, and Allard Schnabel. Nutzung der ekg-signal-datenbank cardiodat der ptb über das internet. In *PTB-XL, a large publicly available electrocardiography dataset*, 2009. URL <https://api.semanticscholar.org/CorpusID:111121953>.
- E Oran Brigham. *The fast Fourier transform and its applications*. Prentice-Hall, Inc., 1988.
- MJ Burke and M Nasor. Wavelet based analysis and characterization of the ecg signal. *Journal of Medical Engineering & Technology*, 28(2):47–55, 2004.
- Chris U. Carmona, François-Xavier Aubet, Valentin Flunkert, and Jan Gasthaus. Neural contextual anomaly detection for time series, 2021. URL <https://arxiv.org/abs/2107.07702>.
- Sidhartha Chaudhury, Chenggang Yu, Ruifeng Liu, Kamal Kumar, Samantha Hornby, Christopher Duplessis, Joel M Sklar, Judith E Epstein, and Jaques Reifman. Wearables detect malaria early in a controlled human-infection study. *IEEE Transactions on Biomedical Engineering*, 69(6): 2119–2129, 2021.
- Chun-Fu Chen, Quanfu Fan, and Rameswar Panda. Crossvit: Cross-attention multi-scale vision transformer for image classification, 2021.
- Moajjem Hossain Chowdhury, Md Nazmul Islam Shuzan, Muhammad EH Chowdhury, Zaid B Mahub, M Monir Uddin, Amith Khandakar, and Mamun Bin Ibne Reaz. Estimating blood pressure from the photoplethysmogram signal and demographic features using machine learning techniques. *Sensors*, 20(11):3127, 2020.
- Se Young Chun, Jae-Hwan Kang, Hanvit Kim, Chungho Lee, Ian Oakley, and Sung-Phil Kim. Ecg based user authentication for wearable devices using short time fourier transform. In *2016 39th international conference on telecommunications and signal processing (tsp)*, pp. 656–659. IEEE, 2016.
- Muhammad Najam Dar, Amna Rahim, Muhammad Usman Akram, Sajid Gul Khawaja, and Aqsa Rahim. Yaad: young adult’s affective data using wearable ecg and gsr sensors. In *2022 2nd International Conference on Digital Futures and Transformative Technologies (ICoDT2)*, pp. 1–7. IEEE, 2022.
- Jacob Devlin, Ming-Wei Chang, Kenton Lee, and Kristina Toutanova. Bert: Pre-training of deep bidirectional transformers for language understanding, 2019. URL <https://arxiv.org/abs/1810.04805>.
- Alexey Dosovitskiy, Lucas Beyer, Alexander Kolesnikov, Dirk Weissenborn, Xiaohua Zhai, Thomas Unterthiner, Mostafa Dehghani, Matthias Minderer, Georg Heigold, Sylvain Gelly, et al. An image is worth 16x16 words: Transformers for image recognition at scale. *arXiv preprint arXiv:2010.11929*, 2020.
- Amirhossein Esmaili, Mohammad Kachuee, and Mahdi Shabany. Nonlinear cuffless blood pressure estimation of healthy subjects using pulse transit time and arrival time. *IEEE Transactions on Instrumentation and Measurement*, 66(12):3299–3308, 2017.
- Navid Mohammadi Foumani, Chang Wei Tan, Geoffrey I Webb, and Mahsa Salehi. Improving position encoding of transformers for multivariate time series classification. *Data Mining and Knowledge Discovery*, 38(1):22–48, 2024.

-
- Freepik. Icons, n.d. URL prefix: <https://www.flaticon.com/free-icon/> , IDs: hypertension_4939229; blood-pressure-gauge_3184052; motion-sensor_2818201; student-sleeping-in-class_43739; diabetes_2750352; blood-cells_3400003; edge-computing_11068838; galvanic-skin-response_11228469; motion-sensor_17881894; accelerometer-sensor_11330476; eeg_9851782; consolidate_5288474; cardiology_12243701; fatigue_2788981; brain_9510259; epilepsy_9836857; cerebrovascular_10281933; arm_5800191.
- A. L. Goldberger, L. A. N. Amaral, L. Glass, J. M. Hausdorff, P. Ch. Ivanov, R. G. Mark, J. E. Mietus, G. B. Moody, C.-K. Peng, and H. E. Stanley. PhysioBank, PhysioToolkit, and PhysioNet: Components of a new research resource for complex physiologic signals. *Circulation*, 101(23):e215–e220, 2000. Circulation Electronic Pages: <http://circ.ahajournals.org/content/101/23/e215.full> PMID:1085218; doi: 10.1161/01.CIR.101.23.e215.
- Tara Hassani. Federated emotion recognition with physiological signals-gsr, 2021.
- Kaiming He, Xinlei Chen, Saining Xie, Yanghao Li, Piotr Dollár, and Ross Girshick. Masked autoencoders are scalable vision learners, 2021. URL <https://arxiv.org/abs/2111.06377>.
- Asmaa Hosni and Mohamed Atef. Remote real-time heart rate monitoring with recursive motion artifact removal using ppg signals from a smartphone camera. *Multimedia Tools and Applications*, 82(13):20571–20588, 2023.
- Kun Hu, Plamen Ch Ivanov, Zhi Chen, Pedro Carpena, and H Eugene Stanley. Effect of trends on detrended fluctuation analysis. *Physical Review E*, 64(1):011114, 2001.
- Po-Yao Huang, Hu Xu, Juncheng Li, Alexei Baevski, Michael Auli, Wojciech Galuba, Florian Metze, and Christoph Feichtenhofer. Masked autoencoders that listen, 2023. URL <https://arxiv.org/abs/2207.06405>.
- Eric Jang, Shixiang Gu, and Ben Poole. Categorical reparameterization with gumbel-softmax, 2017.
- Ian T Jolliffe and Jorge Cadima. Principal component analysis: a review and recent developments. *Philosophical transactions of the royal society A: Mathematical, Physical and Engineering Sciences*, 374(2065):20150202, 2016.
- Mohammad Kachuee, Mohammad Mahdi Kiani, Hoda Mohammadzade, and Mahdi Shabany. Cuffless blood pressure estimation algorithms for continuous health-care monitoring. *IEEE Transactions on Biomedical Engineering*, 64(4):859–869, 2016.
- Diederik P Kingma and Max Welling. Auto-encoding variational bayes, 2022. URL <https://arxiv.org/abs/1312.6114>.
- Pranesh Krishnan, Sazali Yaacob, Annapoorni Pranesh Krishnan, Mohamed Rizon, and Chun Kit Ang. Eeg based drowsiness detection using relative band power and short-time fourier transform. *J. Robotics Netw. Artif. Life*, 7(3):147–151, 2020.
- Yongbo Liang, Zhencheng Chen, Guiyong Liu, and Mohamed Elgendi. A new, short-recorded photoplethysmogram dataset for blood pressure monitoring in china. *Scientific data*, 5(1):1–7, 2018. doi: 10.6084/m9.figshare.5459299.v5.
- Che Liu, Zhongwei Wan, Sibao Cheng, Mi Zhang, and Rossella Arcucci. Etp: Learning transferable ecg representations via ecg-text pre-training. In *ICASSP 2024-2024 IEEE International Conference on Acoustics, Speech and Signal Processing (ICASSP)*, pp. 8230–8234. IEEE, 2024.
- George Mathew, Daniel Barbosa, John Prince, and Subramaniam Venkatraman. Foundation models for cardiovascular disease detection via biosignals from digital stethoscopes. *npj Cardiovascular Health*, 1(1):25, Oct 2024. ISSN 2948-2836. doi: 10.1038/s44325-024-00027-5. URL <https://doi.org/10.1038/s44325-024-00027-5>.

-
- Temesgen Mehari and Nils Strodthoff. Self-supervised representation learning from 12-lead ecg data. *Computers in Biology and Medicine*, 141:105114, February 2022. ISSN 0010-4825. doi: 10.1016/j.compbio.2021.105114. URL <http://dx.doi.org/10.1016/j.compbio.2021.105114>.
- Gatis Mikelsons, Matthew Smith, Abhinav Mehrotra, and Mirco Musolesi. Towards deep learning models for psychological state prediction using smartphone data: Challenges and opportunities. In *MLAH Workshop at 31st Conference on Neural Information Processing Systems (NIPS)*, 2017. URL <https://arxiv.org/abs/1711.06350>.
- Jianliang Min, Ping Wang, and Jianfeng Hu. The original EEG data for driver fatigue detection. *figshare.Dataset.*, 7 2017. doi: 10.6084/m9.figshare.5202739.v1.
- Mostafa Neo Mohsenvand, Mohammad Rasool Izadi, and Pattie Maes. Contrastive representation learning for electroencephalogram classification. In Emily Alsentzer, Matthew B. A. McDermott, Fabian Falck, Suproteem K. Sarkar, Subhrajit Roy, and Stephanie L. Hyland (eds.), *Proceedings of the Machine Learning for Health NeurIPS Workshop*, volume 136 of *Proceedings of Machine Learning Research*, pp. 238–253. PMLR, 11 Dec 2020. URL <https://proceedings.mlr.press/v136/mohsenvand20a.html>.
- Muhammad Muzammil. Finetuning endevsols/tinylama-2.5t-clinical model on clinical dataset., 2021. URL <https://huggingface.co/muzammil-eds/tinylama-2.5T-Clinical-v2>.
- Anna Nedorubova, Alena Kadyrova, and Aleksey Khlyupin. Human activity recognition using continuous wavelet transform and convolutional neural networks. *arXiv preprint arXiv:2106.12666*, 2021a.
- Anna Nedorubova, Alena Kadyrova, and Aleksey Khlyupin. Human activity recognition using continuous wavelet transform and convolutional neural networks. *arXiv preprint arXiv:2106.12666*, 2021b.
- Pranshu Cbs Negi, Himanshu Giri, Shiru Sharma, Neeraj Sharma, et al. A comparative study of scalograms for human activity classification. In *2024 IEEE 4th International Conference on Human-Machine Systems (ICHMS)*, pp. 1–5. IEEE, 2024.
- Yuqi Nie, Nam H. Nguyen, Phanwadee Sinthong, and Jayant Kalagnanam. A time series is worth 64 words: Long-term forecasting with transformers, 2023. URL <https://arxiv.org/abs/2211.14730>.
- Joon Sung Park, Joseph C. O’Brien, Carrie J. Cai, Meredith Ringel Morris, Percy Liang, and Michael S. Bernstein. Generative agents: Interactive simulacra of human behavior, 2023.
- Arvind Pillai, Dimitris Spathis, Fahim Kawsar, and Mohammad Malekzadeh. Papagei: Open foundation models for optical physiological signals, 2024. URL <https://arxiv.org/abs/2410.20542>.
- Bo Qian and Khaled Rasheed. Hurst exponent and financial market predictability. In *IASTED conference on Financial Engineering and Applications*, pp. 203–209. Proceedings of the IASTED International Conference Cambridge, MA, 2004.
- Alec Radford, Jong Wook Kim, Chris Hallacy, Aditya Ramesh, Gabriel Goh, Sandhini Agarwal, Girish Sastry, Amanda Askell, Pamela Mishkin, Jack Clark, Gretchen Krueger, and Ilya Sutskever. Learning transferable visual models from natural language supervision, 2021. URL <https://arxiv.org/abs/2103.00020>.
- Schmidt Philip Reiss Attila, Indlekofer Ina. PPG-DaLiA. UCI Machine Learning Repository, 2019. DOI: <https://doi.org/10.24432/C53890>.
- Jorge Reyes-Ortiz, Davide Anguita, Alessandro Ghio, Luca Oneto, and Xavier Parra. Human Activity Recognition Using Smartphones. UCI Machine Learning Repository, 2012. DOI: <https://doi.org/10.24432/C54S4K>.

-
- Philip Schmidt, Attila Reiss, Robert Duerichen, Claus Marberger, and Kristof Van Laerhoven. Introducing wesad, a multimodal dataset for wearable stress and affect detection. In *Proceedings of the 20th ACM international conference on multimodal interaction*, pp. 400–408, 2018.
- Artemios-Anargyros Semenoglou, Evangelos Spiliotis, and Vassilios Assimakopoulos. Image-based time series forecasting: A deep convolutional neural network approach. *Neural Networks*, 157: 39–53, 2023. ISSN 0893-6080. doi: <https://doi.org/10.1016/j.neunet.2022.10.006>. URL <https://www.sciencedirect.com/science/article/pii/S0893608022003902>.
- Roshwin Sengupta, Ilia Polian, and John P Hayes. Wavelet transform assisted neural networks for human activity recognition. In *2022 IEEE International Symposium on Circuits and Systems (ISCAS)*, pp. 1254–1258. IEEE, 2022.
- Gašper Slapničar, Nejc Mlakar, and Mitja Luštrek. Blood pressure estimation from photoplethysmogram using a spectro-temporal deep neural network. *Sensors*, 19(15):3420, 2019.
- Dimitris Spathis, Ignacio Perez-Pozuelo, Soren Brage, Nicholas J. Wareham, and Cecilia Mascolo. Self-supervised transfer learning of physiological representations from free-living wearable data. In *Proceedings of the Conference on Health, Inference, and Learning, ACM CHIL '21*, pp. 69–78. ACM, April 2021. doi: 10.1145/3450439.3451863. URL <http://dx.doi.org/10.1145/3450439.3451863>.
- John Michael Tutill Thompson, H Bruce Stewart, and Rick Turner. Nonlinear dynamics and chaos. *Computers in Physics*, 4(5):562–563, 1990.
- Christopher Torrence and Gilbert P Compo. A practical guide to wavelet analysis. *Bulletin of the American Meteorological society*, 79(1):61–78, 1998.
- Akhil Vaid, Joy Jiang, Ashwin Sawant, Stamatios Lerakis, Edgar Argulian, Yuri Ahuja, Joshua Lampert, Alexander Charney, Hayit Greenspan, Jagat Narula, Benjamin Glicksberg, and Girish N. Nadkarni. A foundational vision transformer improves diagnostic performance for electrocardiograms. *npj Digital Medicine*, 6(1):108, Jun 2023. ISSN 2398-6352. doi: 10.1038/s41746-023-00840-9. URL <https://doi.org/10.1038/s41746-023-00840-9>.
- Laurens Van der Maaten and Geoffrey Hinton. Visualizing data using t-sne. *Journal of machine learning research*, 9(11), 2008.
- Ashish Vaswani, Noam Shazeer, Niki Parmar, Jakob Uszkoreit, Llion Jones, Aidan N. Gomez, Lukasz Kaiser, and Illia Polosukhin. Attention is all you need, 2023. URL <https://arxiv.org/abs/1706.03762>.
- S Vishnupriya and K. Meenakshi. Automatic music genre classification using convolution neural network. In *2018 International Conference on Computer Communication and Informatics (ICCCI)*, pp. 1–4, 2018. doi: 10.1109/ICCCI.2018.8441340. URL <https://ieeexplore.ieee.org/document/8441340>.
- Christopher Wimmer and Navid Rekabsaz. Leveraging vision-language models for granular market change prediction, 2023. URL <https://arxiv.org/abs/2301.10166>.
- Alan Wolf, Jack B Swift, Harry L Swinney, and John A Vastano. Determining lyapunov exponents from a time series. *Physica D: nonlinear phenomena*, 16(3):285–317, 1985.
- Gerald Woo, Chenghao Liu, Akshat Kumar, Caiming Xiong, Silvio Savarese, and Doyen Sahoo. Unified training of universal time series forecasting transformers, 2024. URL <https://arxiv.org/abs/2402.02592>.
- Yusong Wu, Ke Chen, Tianyu Zhang, Yuchen Hui, Taylor Berg-Kirkpatrick, and Shlomo Dubnov. Large-scale contrastive language-audio pretraining with feature fusion and keyword-to-caption augmentation. In *ICASSP 2023-2023 IEEE International Conference on Acoustics, Speech and Signal Processing (ICASSP)*, pp. 1–5. IEEE, 2023.

-
- Yan Yan, Yi-Chun Huang, Jinjin Zhao, Yu-Shi Liu, Liang Ma, Jing Yang, Xu-Dong Yan, Jing Xiong, and Lei Wang. Topological nonlinear analysis of dynamical systems in wearable sensor-based human physical activity inference. *IEEE Transactions on Human-Machine Systems*, 53(4):792–801, 2023a. doi: 10.1109/THMS.2023.3275774.
- Yan Yan, Yi-Chun Huang, Jinjin Zhao, Yu-Shi Liu, Liang Ma, Jing Yang, Xu-Dong Yan, Jing Xiong, and Lei Wang. Topological nonlinear analysis of dynamical systems in wearable sensor-based human physical activity inference. *IEEE Transactions on Human-Machine Systems*, 53(4):792–801, 2023b. doi: 10.1109/THMS.2023.3275774.
- Hang Yuan, Tatiana Plekhanova, Rosemary Walmsley, Amy C. Reynolds, Kathleen J. Maddison, Maja Bucan, Philip Gehrman, Alex Rowlands, David W. Ray, Derrick Bennett, Joanne McVeigh, Leon Straker, Peter Eastwood, Simon D. Kyle, and Aiden Doherty. Self-supervised learning of accelerometer data provides new insights for sleep and its association with mortality. *npj Digital Medicine*, July 2023. doi: 10.1101/2023.07.07.23292251. URL <http://dx.doi.org/10.1101/2023.07.07.23292251>.
- Hongyi Zhang, Moustapha Cisse, Yann N. Dauphin, and David Lopez-Paz. mixup: Beyond empirical risk minimization, 2017.
- Wenrui Zhang, Ling Yang, Shijia Geng, and Shenda Hong. Self-supervised time series representation learning via cross reconstruction transformer. *IEEE Transactions on Neural Networks and Learning Systems*, 2023a.
- Xiang Zhang, Ziyuan Zhao, Theodoros Tsiligkaridis, and Marinka Zitnik. Self-supervised contrastive pre-training for time series via time-frequency consistency. *Advances in Neural Information Processing Systems*, 35:3988–4003, 2022.
- Xiao Zhang, Yongqiang Lyu, Tong Qu, Pengfei Qiu, Xiaomin Luo, Jingyu Zhang, Shunjie Fan, and Yuanchun Shi. Photoplethysmogram-based cognitive load assessment using multi-feature fusion model. *ACM Trans. Appl. Percept.*, 16(4), September 2019. ISSN 1544-3558. doi: 10.1145/3340962. URL <https://doi.org/10.1145/3340962>.
- Xiyuan Zhang, Ranak Roy Chowdhury, Jiayun Zhang, Dezhi Hong, Rajesh K. Gupta, and Jingbo Shang. Unleashing the power of shared label structures for human activity recognition, 2023b. URL <https://arxiv.org/abs/2301.03462>.
- Xiyuan Zhang, Ranak Roy Chowdhury, Rajesh K Gupta, and Jingbo Shang. Large language models for time series: A survey. *arXiv preprint arXiv:2402.01801*, 2024a.
- Xiyuan Zhang, Diyan Teng, Ranak Roy Chowdhury, Shuheng Li, Dezhi Hong, Rajesh K. Gupta, and Jingbo Shang. Unimts: Unified pre-training for motion time series, 2024b. URL <https://arxiv.org/abs/2410.19818>.

APPENDIX

A RELATED WORK

Self-supervised learning paradigm, coupled with large and diverse datasets, has gained popularity recently due to its adaptability to various downstream tasks (Bommasani et al., 2022). This approach has attracted significant interest in the wearable sensor domain, particularly for applications in physiological signal analysis. Recent studies have utilized self-supervised learning in wearable devices for tasks such as activity recognition (Spathis et al., 2021; Yuan et al., 2023; Zhang et al., 2023b). Additionally, it has been applied to physiological signals such as PPG, ECG, and EEG, spanning various healthcare monitoring tasks (Abbaspourazad et al., 2023; Pillai et al., 2024; Zhang et al., 2019; Mehari & Strothoff, 2022; Mohsenvand et al., 2020). However, these studies often rely on a predefined set of devices, which limits the models’ adaptability when clinical application settings change. For instance, when new devices or modalities are introduced, these models, which have not been exposed to such data during training, often require fine-tuning to remain functional. Furthermore, many of these models are not publicly accessible due to the sensitivity of healthcare data, which hinders progress in this area. These challenges underscore the need for an open, pre-trained model that can accommodate various device configurations and adapt to evolving clinical requirements.

On the other hand, general time series models (Ansari et al., 2024; Woo et al., 2024; Zhang et al., 2022) have shown significant advancements but are predominantly trained and evaluated in domains such as transportation, energy consumption, and finance, with limited exploration in physiological signals. While physiological signals are inherently multivariate time series, these models have not been trained on such data, leaving their transferability to the physiological sensor domain uncertain. Ignoring the correlations between different sensors may result in suboptimal performance when applied to this domain. Motivated by these limitations, this work focuses on developing a foundation model for sensory time series data capable of accommodating arbitrary combinations of device modalities as multivariate series, while investigating strategies to effectively leverage sensor correlations.

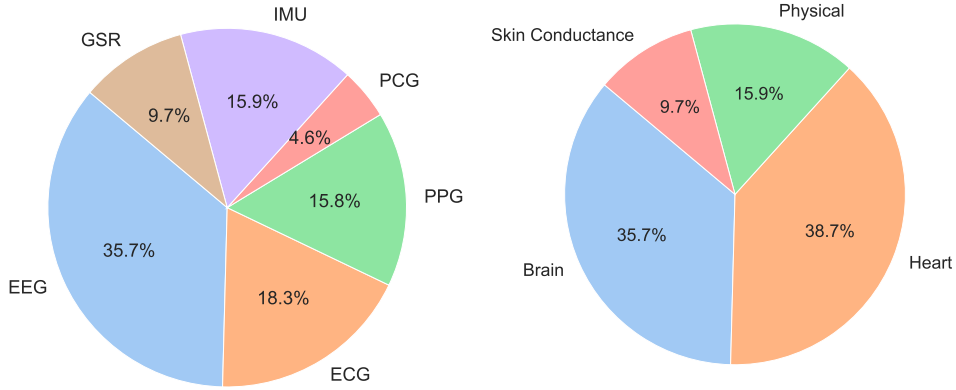
B IMPLEMENTATION DETAIL

Datasets. Few openly accessible multi-channel or multi-device datasets for physiological signals exist, limiting advancements in this field. To address this gap, we curated a dataset comprising approximately 385 hours of recordings. Using the augmentation algorithm described below, we expanded this dataset to 4294 hours. The distribution of the pretraining dataset, as shown in Figure 7, reflects the inherent diversity of the original recordings, ensuring balanced representation across channels and devices. This curated and augmented dataset provides a critical resource for developing robust models, facilitating progress in multi-channel physiological signal research.

Data Preprocess. For the data preparation, we set the uniform sampling rate and interval length to 65 HZ and 6 seconds respectively. In our case, 65 Hz covers most of the frequency bands of interest such as heart activity, physical motions, and neuron activity up to the beginning of Gamma power (above 30 Hz). And a great amount of samples are less than 6 seconds such as (Reyes-Ortiz et al., 2012; Liang et al., 2018; Bousseljot et al., 2009). We conduct basic pre-processing for each signal with identical setting: (1) de-trended by subtract the result of a linear least-squares fit to series data from the raw time series, and (2) Gaussian smoothed with standard deviation of 1.3 (0.02 seconds), ensuring a highly consistent dataset for training.

Since the Transformer’s computational requirements scale quadratically with input length, to release the full potential of our self-supervised algorithm, we segment our multivariate time series into intervals with a uniform length and pad shorter samples with zeros. This approach not only enables parallel processing of samples in large minibatches but also addresses variation in the length of individual samples.

For the downstream task, we split the data into train and test sets for linear probing evaluation with portion of 80% and 20% correspondingly. The split is stratified on the anonymized subject ID if this information is provided by the dataset.



(a) Distribution of sensor signals for pretrain. (b) Distribution of type of information for pretrain.

Figure 7: Pretrain data distribution.

Data Augmentation. Since there are very few publicly available datasets containing multiple devices or modalities, we aim to expand our curated training set to fully leverage the potential of self-supervised learning. Inspired by data augmentation techniques in computer vision and natural language processing (Zhang et al., 2017; Carmona et al., 2021), we adopt a heuristic approach to augment the dataset. Specifically, we augment each sub-dataset by a factor of 10. For each dataset, we sample two time series, randomly extract a segment from one, and substitute it with a transformed counterpart, as outlined in the pseudocode in Algorithm 1. As a result, our training set is expanded to 2,586,404 segments, corresponding to 4,294 hours of data.

Algorithm 1 Time Series Mixup Augmentation

Input: Time series dataset \mathcal{X} , number of augmentations n

Output: Augmented Dataset $\tilde{\mathcal{X}}$

- 1: **for** $i = 1$ to n **do**
- 2: Sample two time series $\mathbf{x}^{(1)}, \mathbf{x}^{(2)} \sim \mathcal{X}$
- 3: Sample a chunk size $\lambda \sim \mathcal{U}(0, l)$
- 4: Sample start indices $s_1, s_2 \sim \mathcal{U}(0, l - \lambda)$
- 5: Swap chunk from $\mathbf{x}^{(2)}$ into $\mathbf{x}^{(1)}$:

$$\mathbf{x}_{s_1:s_1+\lambda}^{(1)} \leftarrow \mathbf{x}_{s_2:s_2+\lambda}^{(2)}$$

- 6: Append $\mathbf{x}^{(1)}$ into $\tilde{\mathcal{X}}$
 - 7: **end for**
 - 8: **return** $\tilde{\mathcal{X}}$
-

Pretraining Framework. Normwear is derived from the Masked Autoencoder (MAE) (He et al., 2021). The detailed hyper-parameter choice is describe in 6. We use a Conv2D layer with a kernel size of (9, 5) and a stride of (9, 5), ensuring no overlapping patches. This layer takes input with 3 channels and projects it to 768 channels, matching the hidden size of our encoders. In Normwear, we apply structured masking independently to each variate along both the frequency and time axes, with respective masking ratios of 0.6 and 0.5. This results in an expected overall masking ratio of 0.8 for each variate. Only the unmasked tokens are passed to the encoder, reducing computational complexity. To enhance representation learning, we introduce six additional transformer blocks as fusion layers, interleaved with the original 12 encoder blocks, creating a total of 18 blocks. Each transformer block has a hidden dimension of 768 and uses LayerNorm as in the original MAE. The latent embeddings obtained from the encoder are projected from 768 to 512 dimensions. Learnable masked tokens are reinserted at their original positions, and positional embeddings are added to guide the decoder in reconstructing the input series. The lightweight decoder consists of two trans-

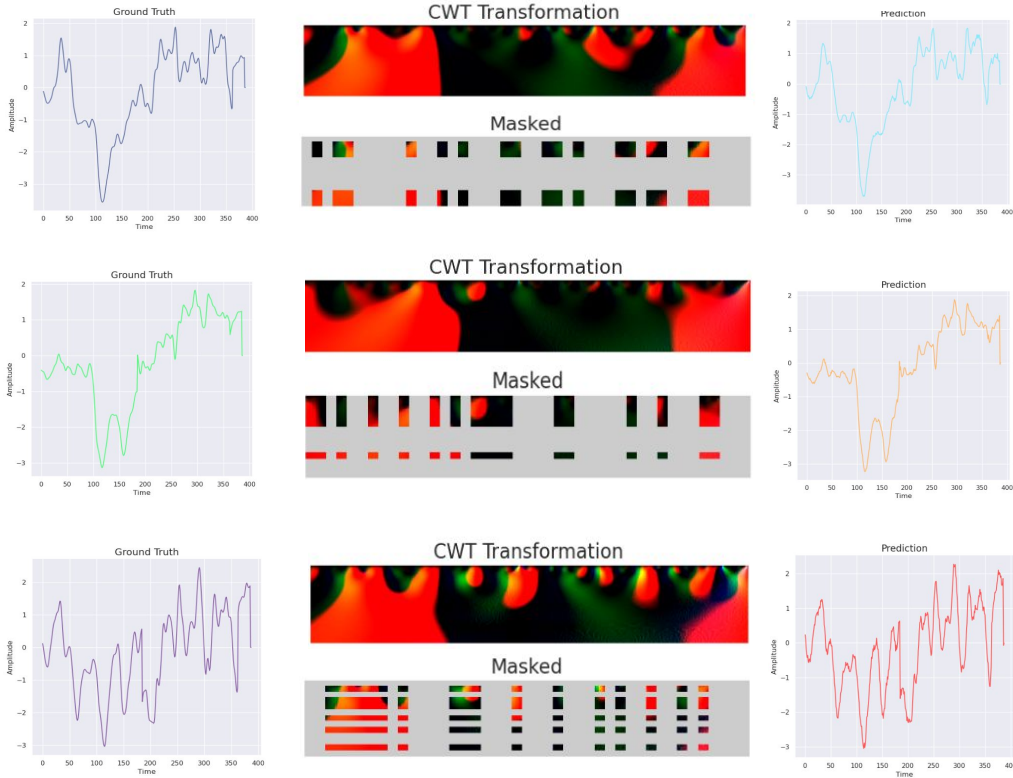


Figure 8: Visualization of original time series, CWT transformation image with structured masking, and reconstructed time series.

former blocks with a hidden dimension of 512, followed by two Conv1D layers. The first Conv1D layer maps from the flattened multivariate signal embedding to an intermediate dimension, and the second Conv1D layer maps from this intermediate dimension back to the original multivariate signal space. A GELU activation function is used between these layers, with BatchNorm applied to the input. The decoder reconstructs the original input series, and the model is trained using Mean Squared Error (MSE) loss on all data points. Our models are pre-trained for 45,000 steps with a batch size of 256, using the AdamW optimizer with a learning rate of 10^{-4} . We did not perform on-the-fly data augmentation, as suggested in the MAE framework, due to the high masking ratio. (An end-to-end example of the input and output of this pretraining pipeline is illustrated in Fig. 8)

MSiTF. For pretraining the representation alignment module, we have the training hyper-parameters in Table 7.

Sentence template example for signal-sext alignment.

- Emotion Task:
 - 'The emotion detected is {}.',
 - 'This subject is feeling {}.',
 - 'The emotional state is {}.',
 - 'The identified emotion is {}.'
- Activity Task:
 - 'This subject is currently {}.',
 - 'The subject is engaged in {}.',
 - 'Current activity is {}.',
 - 'Subjects activity is {}.'

where $\{\}$ is the placeholder for the corresponding label of each sample in pretraining datasets.

Statistical Feature list:

Features in *time domain*: mean, std, max, min, skew, kurtosis, 25% quantile, median, 75% quantile.

Features in *frequency domain*: centroid, spread, mean frequency, peak frequency, 25% quantile frequency, median frequency, 75% quantile frequency.

Radar Plot or Performance Trend. To enhance the visual contrast between model performances across tasks, we applied the Softmax function to the raw performance scores. This transformation rescales the scores to a range between 0 and 1, accentuating relative differences between models. While the Softmax transformation emphasizes the relative improvement of our model over others, we note that the absolute scores may differ from those originally reported.

Table 6: NormWear Pretraining Hyper-parameters.

Hyper-parameter	Value
# cross-patches Transformer Encoder	12
# cross-channels Transformer Encoder	6
# Transformer Decoder	2
# Attention Heads	12
Encoder Latent Size	768
Decoder Latent Size	512
Feedforward Latent Size	3072
Normalization	LayerNorm
Patch size (time axis)	9
Patch size (scale axis)	5
Optimizer	AdamW
Loss Scalar	NativeScaler
Base Learning Rate (blr)	1e-3
Epochs	140
Batch size	192

Table 7: MSiFT Hyper-parameter

Hyper-parameter	Value
Learning rate (lr)	1e-3
Epochs	40
Batch size	32
L2 regularization	5e-6
lr decay rate	0.997
λ	0.5
τ	0.5

C COMPLEXITY ANALYSIS OF DIFFERENT APPROACHES FOR CROSS-CHANNEL FUSION

When conducting multi-channel modeling, for example, when the input comprises an arbitrary number of signals, a fusion operation needs to be conducted across all channels in order to let the model extract correlation information. Because we will deploy the model on an edge device like Jetson Nano, other than empirical evidence of the performance, we also have to consider the computation complexity of different approaches. A brief visualization of the runtime complexity of different approaches is presented in figure 9. The detailed derivation is presented in the following subsections.

C.1 ALL-ATTENTION

For the approach of conducting self-attention by concatenating all the patches, we arrive the Big-O complexity expression as follows:

- We denote C as the number of input channels, d as the embedding size, L as the number of patches convolved from the time series in each channel (proportional to sequence length), and $x \in \mathbb{R}^{C \times L \times d}$ as the input data before feeding into the fusion block. We have a total of $L \cdot C$ patches.
- When calculating the attention scores, dot products are computed for each pair of the patches, which results in the following calculation process:

$$\begin{aligned} &\text{for } i \text{ in } [1, 2, \dots, C] \text{ do} \\ &\quad \text{for } j \text{ in } [1, 2, \dots, L] \text{ do} \\ &\quad\quad 2) N = \exp(\text{attn}(x_{i,j})), \implies O(L \cdot C) \end{aligned}$$

```

for  $k$  in  $[1, 2, \dots, C]$  do
  for  $l$  in  $[1, 2, \dots, L]$  do
    1) Calculate dot product:  $\text{attn}(x_{i,j}, x_{k,l}) = x_{i,j}^T x_{k,l}, \implies O(2d)$ 
    2) Softmax over all-attention scores,  $\frac{\exp(\text{attn}(x_{i,j}, x_{k,l}))}{N}, \implies O(1)$ 
    3) Weighted Average:  $x_{i,j} + \text{attn}(x_{i,j}, x_{k,l}) \cdot x_{k,l}, \implies O(2d)$ 
  end for
end for
end for
end for

```

where "1), 2), 3)" represents the operations conducted at the first, second, and third rounds of entering the entire nested loops. The complexity for the first round of operation results in a complexity of:

$$\sum_{i=1}^C \sum_{j=1}^L \sum_{k=1}^C \sum_{l=1}^L 2d = \sum_{i=1}^C \sum_{j=1}^L \sum_{k=1}^C L \cdot 2d = \sum_{i=1}^C \sum_{j=1}^L C \cdot L \cdot 2d = O(d \cdot (L \cdot C)^2) \quad (3)$$

where in the case of multi-head attention, the dot product still has the complexity of $O(2d)$, and because the number of heads is a constant, the final complexity is equivalent to the result in equation 3.

- Similarly, the softmax operation will result in a complexity of $O((L \cdot C)^2)$, and the final weighted average operation will also have a complexity of $O(d \cdot (L \cdot C)^2)$, which results in total complexity of

$$O(d \cdot (L \cdot C)^2) + O((L \cdot C)^2) + O(d \cdot (L \cdot C)^2) = O(d \cdot (L \cdot C)^2) \quad (4)$$

C.2 CROSS-ATTENTION

For the pairwise cross-attention approach following guidance of Chen et al. (2021), we have the operation defined as

```

for  $i$  in  $[1, 2, \dots, C - 1]$  do
  for  $j$  in  $[1, 2, \dots, C]$  do
    2)  $N = \exp(\text{attn}(x_{i,1}))$ ,  $\implies O(L)$ 
    for  $k$  in  $[2, 3, \dots, L]$  do
      1) Calculate  $\text{attn}(x_{i,1}, x_{j,k})$ ,  $\implies O(2d)$ 
      2) Softmax over all-attention scores,  $\frac{\exp(\text{attn}(x_{i,1}, x_{j,k}))}{N}$ ,  $\implies O(1)$ 
      3) Weighted average:  $x_{i,1} + x_{j,k}$ ,  $\implies O(2d)$ 
    end for
  end for
end for

```

with the same notion in the previous subsection. The total complexity is

$$O(C^2 \cdot L \cdot 2d) + O(C^2 \cdot L) + O(C^2 \cdot L \cdot 2d) = O(d \cdot L \cdot C^2) \quad (5)$$

C.3 [CLS]-ATTENTION

This is the approach that we adopted for the final version of our proposed foundation model. Only the embedding corresponding to the [CLS] token of each channel is involved during the self-attention operation. Therefore, the complexity is

$$O(d \cdot C^2) \quad (6)$$

C.4 MEAN-POOL ATTENTION

For fusion with mean-pool attention, we first calculate the mean representation for each channel, resulting in a complexity of $O(C \cdot L \cdot d)$. And self-attention with these mean representations has the same complexity as [CLS]-attention, which is $O(d \cdot C^2)$. Thus, the total complexity is

$$O(C \cdot L \cdot d) + O(d \cdot C^2) = O(d \cdot (L \cdot C + C^2)) \quad (7)$$

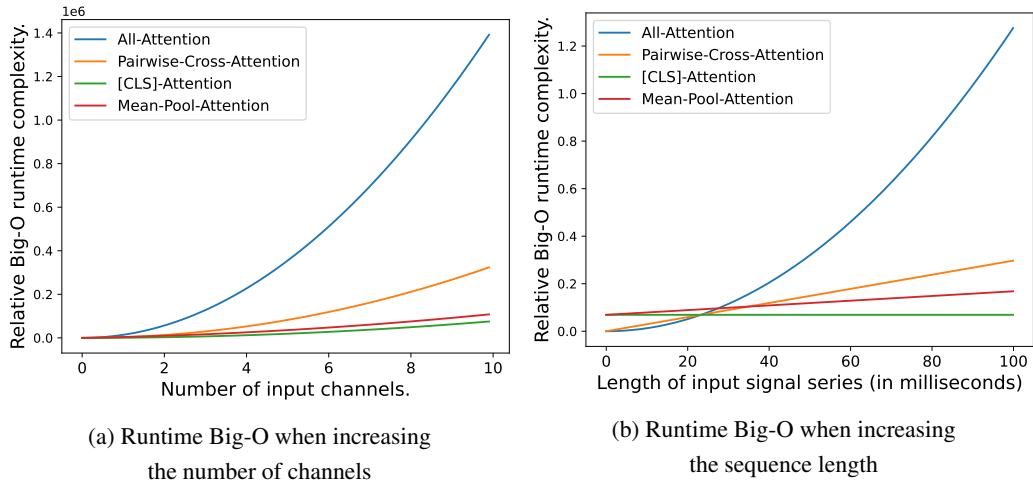


Figure 9: Visualization of runtime complexity when scaling up the number of channels or the sequence length.

D ABLATION STUDY

Due to computational constraints, we will conduct the ablation study on our smaller dataset (37k samples) to train and evaluate the model, establishing a proof of concept and demonstrating the effectiveness of our approach in a controlled setting.

Fusion Schemes. Table 8 shows the performance of different fusion schemes, including (1) no fusion, (2) cross-attention fusion, (3) [CLS]-attention fusion, and (4) mean-pooling fusion. We excluded all-attention fusion in our ablation study because it is computationally prohibitive. Among all the compared strategies, the [CLS] token fusion generally achieves the best accuracy with a minor increase in parameters.

Table 8: Performance Comparison of Various Fusion Schemes

Downstream Tasks	No fusion	Cross-Attention fusion	Mean pooling fusion	[CLS] Token fusion
WESAD	72.209	74.165	71.99	75.390
UCI-HAR	97.793	96.908	97.566	98.928
DriverFatigue	73.252	60.308	72.552	75.167
Activity Recognition Avg.	81.085	77.127	80.703	83.162
Epilepsy (eye open)	90.966	84.075	89.817	92.203
Epilepsy (eye close)	94.399	93.589	93.912	94.908
Epilepsy (health area)	87.866	86.899	87.248	88.117
Epilepsy (tumor area)	86.599	86.861	87.152	86.888
Epilepsy (seizure)	97.477	96.351	96.719	96.638
GAMEEMO	57.695	56.724	58.079	56.532
EEG Main Tasks Avg.	85.834	84.083	85.488	85.881
ECG-Abnormal	99.429	99.441	99.268	99.041
PPG-BP (HTN)	61.850	60.983	63.577	60.344
PPG-BP (DM)	58.333	62.800	62.200	59.459
PPG-BP (CVA)	61.319	61.458	59.236	70.278
PPG-BP (CVD)	48.417	53.585	46.961	52.596
PhysioNet EMG	93.715	95.49	86.749	98.184
Risk Evaluation Avg.	70.511	72.293	69.665	73.317
Noninvasive-BP	88.356	92.759	88.719	92.470
PPG-Hgb	95.031	93.413	95.086	94.766
Fetal-fPCG	98.582	99.145	98.771	99.088
Vital Signs Avg.	93.990	95.106	94.192	95.441
Micro Avg.	81.294	80.831	80.867	82.833
Macro Avg.	82.855	82.152	82.512	84.450

Masking Strategies in Pre-training. We ablated our masking strategy introduced in Section 2.3. Using a consistent mask ratio of 0.8 in all strategies, we found that applying masking along the scale and time axes produced the best performance (details in Table 9).

Table 9: Performance Comparison of Different Masking Strategies

Downstream Tasks	Unstructured Mask ($P = 0.8$)	Time Mask ($P_t = 0.8, P_f = 0.0$)	Scale Mask ($P_t = 0.0, P_f = 0.8$)	Structured Mask ($P_t = 0.6, P_f = 0.5$)
WESAD	71.46	71.952	72.201	75.390
UCI-HAR	97.097	98.438	98.106	98.928
DriverFatigue	72.719	73.424	78.354	75.167
Activity Recognition Avg.	80.425	81.271	82.887	83.162
Epilepsy (eye open)	89.521	91.895	89.407	92.203
Epilepsy (eye close)	93.471	94.808	93.786	94.908
Epilepsy (health area)	86.812	88.510	87.317	88.117
Epilepsy (tumor area)	86.524	88.254	85.502	86.888
Epilepsy (seizure)	96.59	97.791	95.29	96.638
GAMEEMO	58.043	56.770	55.771	56.532
EEG Main Tasks Avg.	85.160	86.338	84.512	85.881
ECG-Abnormal	99.085	99.316	98.296	99.041
PPG-BP (HTN)	58.880	55.333	59.230	60.344
PPG-BP (DM)	61.074	48.386	58.896	59.459
PPG-BP (CVA)	56.389	58.472	64.167	70.278
PPG-BP (CVD)	52.572	46.557	55.666	52.596
PhysioNet EMG	85.160	95.490	83.922	98.184
Risk Evaluation Avg.	68.860	67.259	70.030	73.317
Noninvasive-BP	90.124	90.650	91.152	92.470
PPG-Hgb	95.314	95.055	94.713	94.766
Fetal-fPCG	98.630	99.121	98.926	99.088
Vital Signs Avg.	94.689	94.942	94.930	95.441
Micro Avg.	80.526	80.568	81.150	82.833
Macro Avg.	82.284	82.453	83.090	84.450

Input Representations. Table 10 compares the performance of two input representations: (1) CWT scalogram and (2) raw time series. The CWT scalogram converts the time series into a time-frequency representation, while the raw time series retains the original sensor data. Among the two representations, the model trained on CWT scalograms demonstrates better performance, suggesting that the time-frequency features enhance model accuracy.

From Table 12, we observe that demographic information and representations extracted from wearable signals have their own strength on different tasks, and most of the time, when we concatenate them together, the overall performance will be better. The performance drop in some cases after concatenation, which indicate that there might be some confounding relationship between these two representations, hence further indicated that the information lies in demographic and the wearable representation from NormWear are focused on different aspects. Same observation are observed with arbitrary model checkpoints during pretraining (denoted as Medium and Large marker representing different stage of training when we do the study on increasing the pretrain size.)

E STATISTICAL SIGNIFICANCE ON THE MODEL COMPARISON

We conduct statistical analysis to check the significance of the difference between models’ performance. We first run the downstream evaluation 100 times for each model on all the tasks, without fixing random seed. We observed that the outcomes stay consistent due to the stability of the optimization process.

We then conduct a permutation test, across the results from these 100 runs, to assess whether our method significantly outperforms the baselines. We declare the alternative hypothesis as whether the score (AUC ROC) of NormWear is greater than the baselines in comparison. The reported P value represents the probability of observing a test statistic as extreme as, or more extreme than, the observed difference under the null hypothesis, assuming that the AUC ROC score of NormWear is not greater than the baseline. The results indicate that in nearly all cases, the statistical significance (p-value) is less than 0.01, providing statistical significance evidence of the robustness and

Table 10: Performance Comparison Between CWT Scalogram and Raw Time Series as Inputs.

Downstream Tasks	Raw Series Input	CWT Scalogram Input
WESAD	70.862	75.390
UCI-HAR	97.969	98.928
DriverFatigue	73.854	75.167
Activity Recognition Avg.	80.895	83.162
Epilepsy (eye open)	91.978	92.203
Epilepsy (eye close)	94.781	94.908
Epilepsy (health area)	88.045	88.117
Epilepsy (tumor area)	85.619	86.888
Epilepsy (seizure)	97.722	96.638
GAMEEMO	54.651	56.532
EEG Main Tasks Avg.	85.466	85.881
ECG-Abnormal	97.701	99.041
PPG-BP (HTN)	52.614	60.344
PPG-BP (DM)	62.012	59.459
PPG-BP (CVA)	56.181	70.278
PPG-BP (CVD)	54.812	52.596
PhysioNet EMG	93.756	98.184
Risk Evaluation Avg.	69.513	73.317
Noninvasive-BP	89.850	92.470
PPG-Hgb	93.832	94.766
Fetal-fPCG	98.977	99.088
Vital Signs Avg.	94.220	95.441
Micro Avg.	80.845	82.833
Macro Avg.	82.523	84.450

Table 11: Performance on various downstream wearable-signal-based health related applications under linear probing evaluation using 5 fold cross validation stratified by subject ID (if provided by the data source). In this table, The classification tasks are solved by Newton’s method with conjugate gradient, and the AUC ROC are reported. The regression (noninvasive BP estimate) tasks are solved by Cholesky’s method with closed form solution for ridge regression, and the relative accuracy (1 minus relative error) are reported. All the scores are the higher the better.

Downstream Tasks	Statistical	Chronos	CLAP	TF-C	NormWear-L (Ours)
WESAD	79.992 +- 0.707	83.332 +- 0.841	87.824 +- 0.463	82.701 +- 0.536	89.585 +- 0.683
UCI-HAR	95.602 +- 0.148	91.956 +- 0.256	96.864 +- 0.175	97.382 +- 0.138	98.179 +- 0.06
DriverFatigue	69.614 +- 1.138	72.48 +- 2.848	66.251 +- 0.471	65.026 +- 1.198	68.971 +- 1.32
GAMEEMO	64.281 +- 1.292	56.694 +- 0.878	64.119 +- 0.543	62.925 +- 0.999	67.863 +- 0.72
Noninvasive	92.83 +- 0.386	92.223 +- 0.356	92.612 +- 0.272	88.707 +- 0.622	93.381 +- 0.516
Avg.	80.464 +- 0.734	79.337 +- 1.036	81.534 +- 0.385	79.348 +- 0.699	83.596 +- 0.660

superiority of our approach. In Table 10, we include the results from conducting the statistical test across different task groups (the groups were highlighted with different colors in the tables in main sections) and the total average scores.

We also present the critical difference diagram (CD) to visually compare the performances of multiple models across datasets, highlighting whether their performance differences are statistically significant. In order to achieve CD diagram, we first conduct Friedman Chi square test on the scores achieved by the models across all the downstream tasks, and observe P value of $P \leq .001$, making sure all the models’ performance are coming from different distribution. Then we conduct Conover post hoc test to check the pair-wise model performance difference, where the P values corresponding to NormWear vs. baselines are presented in the last row of Table 10. Finally, we create CD diagram based on these results, and result in the diagram shown in Figure 11. Our proposed model, NormWear is far apart from the bar, indicating its statistical significance against competitive baselines.

Table 12: Checking the reliance on demographic information.

Downstream Tasks	Simple Baseline Mode and Mean	Demographic	NormWear-Medium	Demographic + NormWear-Medium	NormWear-Large	Demographic + NormWear-Large
WESAD	50.000	49.907	74.227	69.06	76.06	68.755
Noninvasive	92.988	92.954	91.427	90.84	92.42	92.528
PPG-Hgb	94.816	95.634	94.911	95.835	94.632	96.384
Fetal-fPCG	99.033	99.039	98.997	99.001	99.072	99.097
Vital Signs Avg.	95.612	95.876	95.112	95.225	95.375	96.003
PPG-BP (HTN)	50.000	59.899	62.746	64.482	62.341	61.291
PPG-BP (DM)	50.000	47.297	62.613	47.86	55.893	60.135
PPG-BP (CVA)	50.000	81.875	67.639	83.681	70.625	77.847
PPG-BP (CVD)	50.000	71.011	51.504	70.37	51.773	67.466
Risk Evaluation Avg.	50.000	65.021	61.126	66.598	60.158	66.685
Micro Avg.	67.105	74.702	75.508	77.641	75.352	77.938
Macro Avg.	65.204	70.268	76.821	76.961	77.198	77.148

Ours/Baselines	Stats	Chronos	CLAP	TFC
NormWear - activity	$P < .01$	$P < .01$	$P < .01$	$P < .01$
NormWear - eeg	$P < .01$	$P < .01$	$P < .01$	$P < .01$
NormWear - risk	$P < .01$	$P < .01$	$P < .01$	$P < .01$
NormWear - vital	$P < .01$	$P < .01$	$P < .01$	$P < .01$
NormWear - micro avg.	$P < .01$	$P < .01$	$P < .01$	$P < .01$
NormWear - macro avg.	$P < .01$	$P < .01$	$P < .01$	$P < .01$
Conover post hoc	$P < .001$	$P < .001$	$P < .001$	$P < .05$

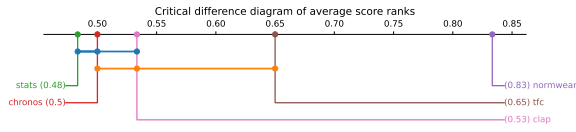


Figure 10: Permutation test on models’ performance.

Figure 11: Critical Difference Diagram

F DEPLOYMENT OF NORMWEAR: TESTING ON THE EDGE

As shown in the table 13, the GPU setup on an NVIDIA RTX 3090 significantly outperforms other configurations in inference speed, achieving an inference time of only 0.18 seconds while maintaining low RAM usage (8.04 MB) and moderate VRAM requirements (732.82 MB). In contrast, the CPU setup on MacOS M1 requires 4.21 seconds, reflecting a considerably slower performance despite similar RAM usage (9.12 MB) and no VRAM consumption. On edge devices, such as the Jetson Nano 4GB, the CPU-based setup exhibits the slowest inference time of 40.69 seconds, while the GPU variant improves this to 34.87 seconds with a VRAM requirement of 504.46 MB. Storage requirements remain constant across all configurations at 1.63 GB.

Table 13: Computation resources consumed across various devices, on 6 channels data for 6 seconds.

Dataset/Task	Infer time	RAM	VRAM	Storage
CPU (MacOS, M1)	4.21 s	9.12 MB	-	1.63 GB
GPU				
- Debian GNU/Linux	0.18 s	8.04 MB	732.82 MB	1.63 GB
- NVIDIA-RTX-3090				
Edge (Jetson Nano 4GB, CPU)	40.69 s	9.12 MB	-	1.63 GB
Edge (Jetson Nano 4GB, GPU)	34.87 s	8.17 MB	504.46 MB	1.63 GB

G FEATURE VISUALIZATION

G.1 THE MODEL IS AGNOSTIC TO THE INPUT SIGNALS

This section investigates whether, without requiring the signal modality type information as input, NORMWEAR can effectively distinguish between different signal sources. We randomly sampled 500 samples for each sensor type and fed them into our pretrained model. We use t-SNE (Van der Maaten & Hinton, 2008), with PCA (Jolliffe & Cadima, 2016) initialization to visualize the learned representations corresponding to the [CLS] special token at the last layer. The PCA preserves the

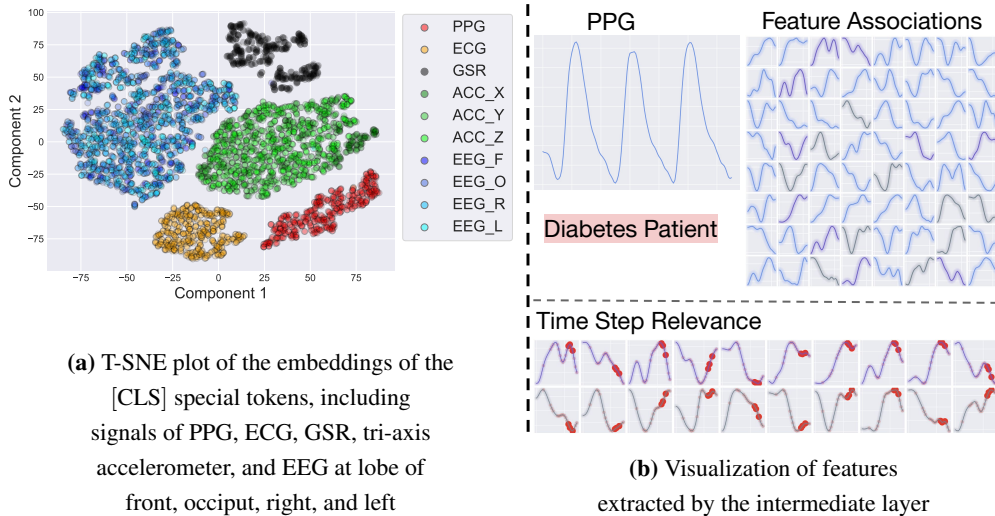


Figure 12: Feature visualization.

global structure, while t-SNE emphasizes local relationships in the data. From Figure 12(a), we observe that representations from sensors located at the same body position are clustered closely together, while representations from different body locations are clearly separated. This suggests that our model is signal-agnostic, as it can recognize the signal type differences, map their representations appropriately in the embedding space, and guide feature extraction within each Transformer block.

G.2 WAVEFORM VISUALIZATION

Figure 12 (b) under “Feature Associations” shows the features extracted by our model. Each patch corresponds to a representation with a vector size of \mathbb{R}^{768} . When ordered by time sequence, these representations form 768 waveforms per layer, representing the model’s extracted features. The figure displays 64 randomly sampled waveforms from a selected layer. The features highlighted in purple and gray indicate the top 10 patterns positively and negatively associated with the target task (diabetes classification, in this example), with associations determined by linear regression parameters during linear probing. Additionally, our relevance-based fusion mechanism identifies the contribution of each time step during inference, highlighted by red dots in the “Time Step Relevance” section of Figure 12 (b).

Such a visualization pipeline can assist researchers and clinicians by offering insights into how the model reaches its final predictions. Given the millions of parameters and hundreds of waveform features per layer, visualizing these features individually is inefficient for understanding the overall behavior of the proposed foundation model. As a result, we use several techniques in nonlinear dynamic analysis (Thompson et al., 1990) to quantify the overall patterns of these extracted features, which are discussed in detail in section 3.5.

G.3 T-SNE PLOT AMONG CLASSES

In this section, we present T-SNE plots of NormWear’s embeddings across different classes to provide insights into their structure and assess their suitability for sample similarity-based information retrieval. It is important to note that these plots are exploratory in nature and do not serve as a claim of the embeddings’ superiority. As shown in Figures 13, 14, 15, clear class separations can be observed in certain scenarios. For example, EEG samples from seizure subjects and normal subjects are distinctly separated, and physical activity types are well-clustered. For ECG data, abnormal heartbeats tend to form cohesive clusters. However, it is essential to recognize that these T-SNE plots reduce the latent representations into a 2D space, which may not fully capture the inherent properties of the embeddings in their original high-dimensional form.

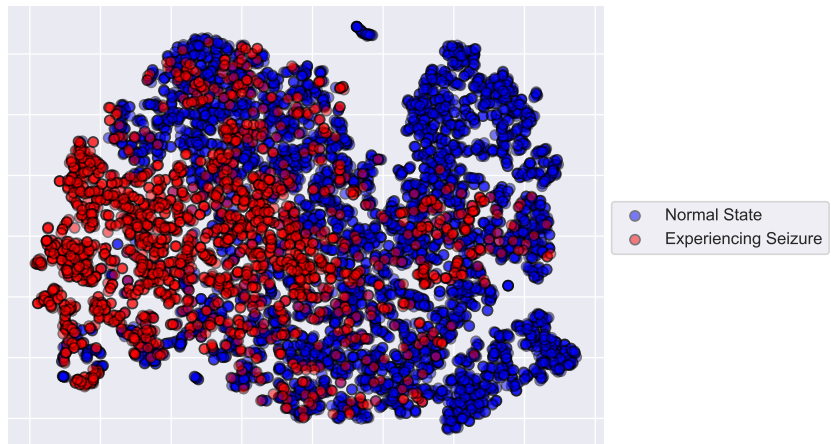


Figure 13: Visualization of embedding on EEG signals.

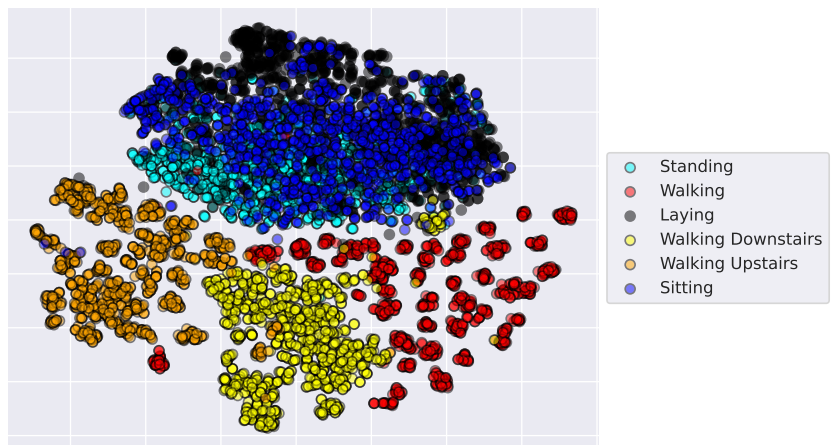


Figure 14: Visualization of embedding on signals from IMU sensors.

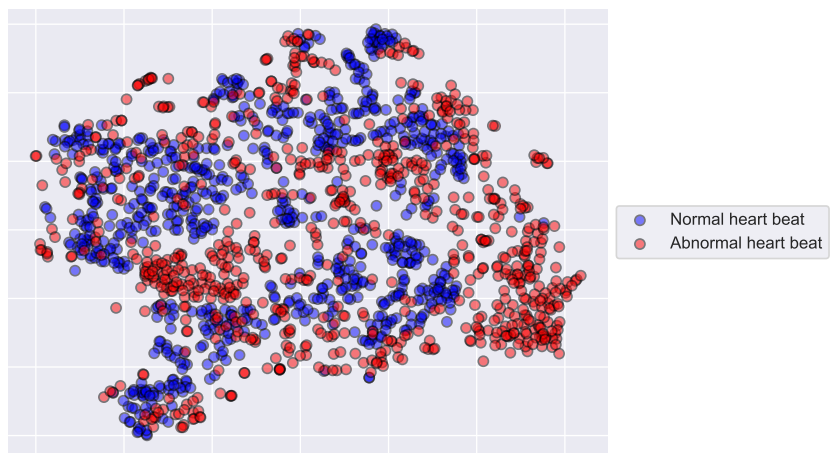


Figure 15: Visualization of embedding of ECG.

H RECONSTRUCTION EXAMPLE

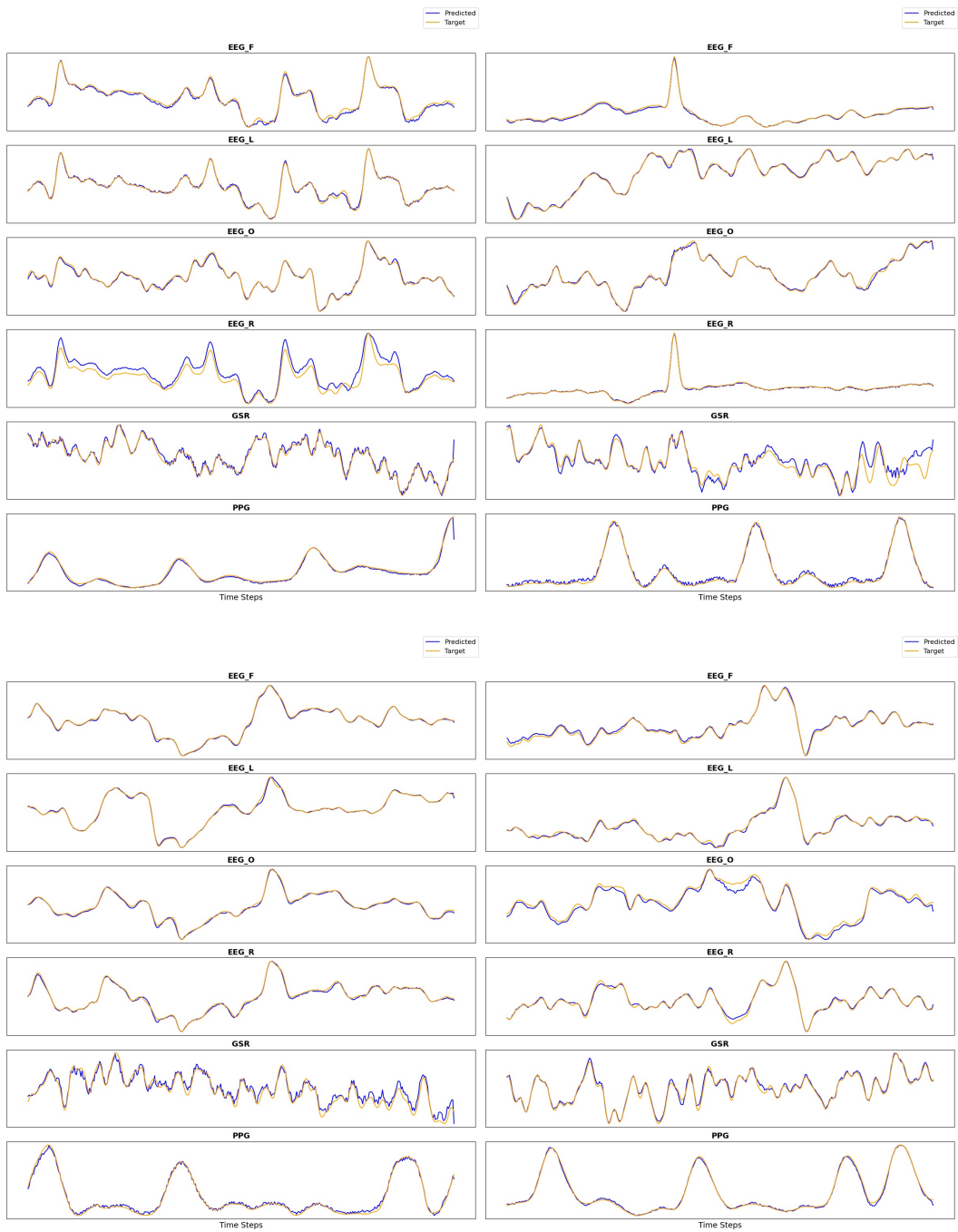


Figure 16: **Uncurated random samples** on Phyatt scalogram, using a NORMWEAR trained in our training set. The masking ratio is 80%.

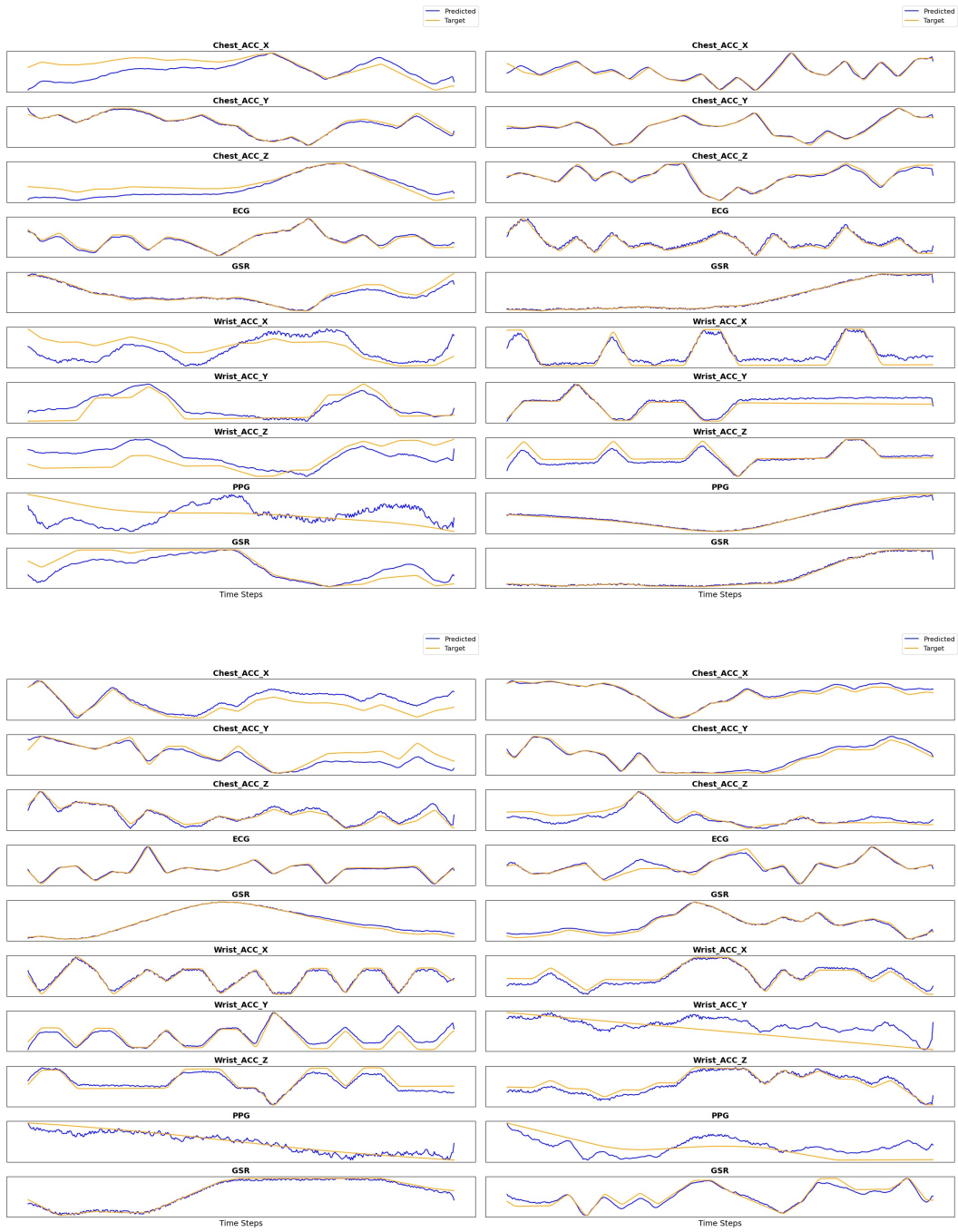


Figure 17: **Uncurated random samples** on WESAD scalogram, using a NORMWEAR trained in our training set. The masking ratio is 80%. Note that the IMU data are not in the training set and, in general, NORMWEAR is able to reconstruct this with high accuracy.